MINIMAL THERMAL FRICTION IN COSMOLOGY

by

Kim V. Berghaus

A dissertation submitted to The Johns Hopkins University in conformity with the requirements for the degree of Doctor of Philosophy.

Baltimore, Maryland

July, 2020

Abstract

Many cosmological datasets contain information about the fundamental building blocks of nature and the forces that govern them. In my research I focus on the connection between particle physics and the evolution of our universe, looking for new physics beyond the Standard Model of particle physics, and beyond ΛCDM, the concordance model of cosmology. The majority of this work explores how a minimal thermal friction mechanism, emerging from first principle particle dynamics, can improve cosmological model building.

In the context of cosmic inflation, I investigate in detail how coupling a rolling axion to a non-Abelian gauge group gives rise to thermal friction, which can alter theoretical predictions for observables in a manner that is consistent with all currently available data while making unique predictions for future data. In particular, the presence of the thermal friction and the resulting thermal bath during inflation suppresses the tensor-to-scalar ratio r, and produces unique non-gaussianities that may be observable within the next ten years in the regime in which thermal friction

is dominant.

I also explore how this minimal thermal friction can address the Hubble tension. A new component added to ΛCDM that behaves like a cosmological constant at early times and then dilutes away as radiation or faster can resolve the Hubble tension. Coupling a rolling axion to a non-Abelian gauge group gives rise to thermal friction which sources a thermal bath. I show that the coupled system of rolling axion and thermal bath automatically exhibits the characteristic behavior of the extra components that are able to resolve the Hubble tension at the background level. These characteristics make this model robust to a wide class of scalar field potentials, thus providing a promising candidate for a natural particle-physics model solution to the Hubble tension.

My work additionally considers long lived decaying massive relics as an explanation for the anomalous high energy neutrino flux detected at IceCube. I explore this UV-extension to the Standard model in detail, considering a variety of cosmological data sets, as well as incorporating electroweak corrections, which become important at high energies. For this project I implemented a Monte Carlo simulation, taking into account electroweak showering processes, as well as a cosmological propagation code, capturing modifications to neutrino energy distributions through re-scatterings.

Readers

David E. Kaplan (Primary Advisor)

Marc Kamionkowski

Nadia Zakamska

Nito Kitchloo

Amitabh Basu

Acknowledgments

I am incredibly grateful to my advisor David. E. Kaplan. Thank you for taking a chance on me when I had no prior experience in theoretical physics. Thank you for pushing me to work harder and do better, and for having my back throughout this process. I have learned so much from you, and your way of approaching science with a mix of rigor and creativity will always be a guiding influence on my own journey as a physicist. Thank you for everything you have done for me.

I have also greatly benefited from the leadership of Marc Kamionkowski and Ibrahima Bah. I am lucky to have had you as role models. Marc, I have found invaluable support and resources in your research group, and your encouragement throughout my PhD has made an important difference. Ibou, your active and inclusive effort in shaping the high-energy group changed my PhD experience. Your level-headed advice has helped me overcome many obstacles I encountered in my research progress. Thank you for caring about people as much as research.

Many postdocs helped me on my way to become a physicist, namely Jack Collins,

ACKNOWLEDGMENTS

Kim Boddy, Vivian Poulin, Ryan McMagnus, Tommi Tekanen, and Gustavo Marques Tavares. Jack, I had a lot of fun chasing anomalies with you. Thanks for reminding me why I love physics whenever I got too stressed to remember myself. Kim, thanks for taking me under your wing. Your perspective and wisdom have been a motivation for me to continue my career in physics.

During this PhD I have found friendship and community in my fellow graduate students. Tanvi Karwal and Dan Pfeffer, you guys are my favorite people. Tanvi, I knew we were going to be best friends when I first met you and I am glad you eventually stopped fighting it as well. Dan, you will always be my gym buddy, even if all the gyms are closed. Thanks for taking care of me, and for being my family away from home. My senior office mates, Julian Munoz, Nikhil Anand, and Brooks Kinch, through you guys I learned so much about navigating the graduate student experience successfully, from the value of a nice cup of coffee to leaving the office on a Friday night to hang out together. The companionship I found in our friendships made the first years of my PhD some of the best in my life. Cris Mantilla-Suarez, you have been an amazing friend and I am glad we got to do this together. I hope there will be many more adventures that we get to tackle side by side.

I am so grateful for the support of my family, my partner Jonathan Constantinides, my parents Heino and Francisca Berghaus, and my brother Rafael Berghaus. Jon, having you by my side has allowed me to truly focus on making progress in my

ACKNOWLEDGMENTS

PhD. Thanks for always encouraging me, for making me happy every day, and listening to me tell you about my research for hours. Heino, Francisca, Rafael, nothing could have prepared me better for getting a PhD than keeping up with you. Your living example of hard work and resilience have made you my most important role models.

Dedication

To my incredibly hard working parents Heino and Francisca Berghaus, who raised me to believe I can achieve anything. You inspire me.

Contents

List of Figures

"My goal is simple. It is a complete understanding of the universe, why it is as it is and why it exists at all."

— Stephen Hawking

Chapter 1

Introduction

The study of particle physics aims to illuminate the interplay of the fundamental constituents that make up our world. Over the last hundred years great progress has been made towards a holistic understanding of those constituents and the fundamental forces that govern them, within the frame work of quantum field theory. High-energy particle colliders directly probed these fundamental particles across a wide range of scales, giving rise to the Standard model of particle physics, which unifies the strong force, the weak force, and electromagnetism within a quantum theory [1]. Despite the incredible achievements that were made, there still remain crucial open questions such as how to embed the Standard model in a UV-complete theory, as well as how to account for dark matter [2, 3] and dark energy [4, 5] in a fundamental theory.

My research focuses on the intersection of particle physics and cosmology, the science of the origin and development of the universe, to seek answers to these questions. The evolution of the universe is closely intertwined with its fundamental constituents and the forces they are governed by. With cosmology becoming a precision science [6–14], it is a field with an abundance of data available to gain insight about particle physics.

Measurements of the cosmic microwave background (CMB) [10, 13, 15], remnants of

light emitted when the universe was only 400,000 years old, provide a window directly into the past. Combined with measurements of light element abundances which probe Big Bang Nucleosynthesis (BBN) [6] at even earlier times, and late time astrophysical data [7,9,11,11,12,14], we are able to gain an understanding of the evolution of the universe from its very beginning up to today. In the current scientific picture the universe starts out hot (> 300 MeV) with a quark-gluon plasma that cools as the universe continues to expand. After it has cooled enough for quarks to confine, first protons and neutrons form, and eventually nuclei are created (~ 10 MeV). Those exist within a hot plasma of electrons and photons and neutrinos, which eventually decouple from the rest (~ 1 MeV). Eventually the universe cools enough for electrons and protons to form neutral hydrogen. At that point, photons decouple from the rest, making the CMB a direct probe of those early times. Eventually ($\sim 10^{-3}$ eV) the first stars and small galaxies begin to form that turn into larger galaxies and galaxy clusters that have been around for a long time today ($\sim 10^{-3}$ eV).

These processes occur in an expanding universe whose expansion is governed by its energy content. The concordance model of cosmology, the flat ΛCDM model, successfully describes numerous data-sets with great accuracy [7–10,13,16], by assuming three different types of energy components: radiation, matter, and dark energy in the form of a cosmological constant Λ. Today the radiation component is made up of photons and neutrinos, the matter component consists of the visible baryonic matter we know how to describe within the Standard model of particle physics, and a dominant 'cold dark matter' component, presumably made up by unknown particles with small thermal velocities [1]. Despite there being no observed non-gravitational interaction between dark matter and visible matter, we can deduce its existence and quantity by its gravitational impact on the clustering of galaxies [2,3], as well as from the CMB [10,13,15]. The cosmological constant is a constant energy density with negative pressure that does not change even as the universe expands, unlike the other two components which dilute. If the energy content is dominated by dark energy the universe undergoes a period of accelerated expansion.

For the last 4 billion years our universe has been in such a period. Before that, for about 9.7 billion years it was dominated by its matter content which was preceded by a period of radiation domination. Before radiation domination and BBN, data suggests that the universe also underwent a rapid period of accelerated expansion in which its size expanded by about 60 e-folds. This period, called inflation, could explain why different patches in the

sky, though impossible to have been in causal contact without inflation, have temperature deviations that only differ by 10^{-5}, as well as why the universe is flat to a high degree of accuracy [17, 18]. While the ΛCDM model is mostly successful in understanding the dynamics of the large scale evolution of the universe, it is a phenomenological model which should emerge from a fundamental theory, describing all particles and their interactions. Open questions on how to do that remain, three of which I am addressing in this dissertation.

The first question that I am exploring in chapter 2 is a novel mechanism that embeds inflation in a fundamental particle physics theory in a way that is both consistent with all the current data as well as predictive for future data. This chapter is heavily based on my publication [19], written with coauthors Peter W. Graham and David E. Kaplan.

Inflation can be embedded into a particle physics framework by assuming a scalar field ϕ, the inflaton, that slowly rolls down a potential $V(\phi)$. In that setup the potential energy dominates over the kinetic energy of ϕ, which allows for a period of accelerated expansion. However, due to the field rolling, this model still introduces dynamics that allow for an exit to the period of accelerated expansion. In the simplest picture, the universe is assumed to be empty, only dominated by the slowly rolling scalar field. Due to the slow changes, accelerated expansion can be maintained for a lot of e-folds. Quantum fluctuations of the scalar field seed the small, nearly scale-invariant anisotropies observed in the cosmic microwave background (CMB). The slow-roll also gives an explanation for the approximate scale-invariance. In this example of cold inflation the universe always ends up empty by the end of its 60 e-folds as any initial content would have diluted away, thus requiring 'reheating', the process of filling the universe with matter (or radiation). In its simplest form, this picture is ruled out by the absence of the detection of primordial gravitational waves, though many modifications exist that circumvent those constraints.

My research focuses on a minimal thermal friction mechanism for the rolling field. Thermal friction allows for the inflation picture to change drastically. Allowing for an interaction between the inflaton and other light fields can give rise to a thermal friction which allows for some of the potential energy of the inflaton to convert into thermal energy through particle production. If that process is efficient enough, a steady-state temperature ($T > H$) can be maintained during slow-roll. Rather than inflating a cold universe, the thermal friction gives rise to a finite temperature the entire time, allowing for the possibility

of a smooth exit into a radiation dominated universe. The inflaton perturbations still seed the anisoptropies in the CMB, however the fluctuations are thermal in nature rather than quantum, leading to a suppression of primordial gravitational waves, and allowing for very low-scale inflation.

This qualitatively different picture has theoretical consequences that agree with observations and have appealing aspects from a model building perspective. However, embedding the thermal friction in a simple self-consistent particle framework can be challenging due to thermal backreactions on the inflaton potential. By coupling an axion to a non-Abelian gauge group, which naturally gives rise to a large thermal friction without thermal backreaction, I have found a viable minimal thermal friction model. Chapter 2 describes this model and its impact on observables in detail. Additionally, I present hybrid inflation with an axion-like coupling as a specific model that can easily fit the current cosmological data, while predicting unique non-gaussianities in the regime in which the thermal friction is larger than Hubble friction.

In the following chapter 3, I show how to utilize this minimal thermal friction mechanism to address a different cosmological anomaly, the Hubble tension [11, 20–22]. The Hubble tension is the disagreement between direct late universe measurements of the expansion of the universe [11, 12, 14], and CMB measurements [10, 13, 23], assuming the ΛCDM model. I am demonstrating how a phenomenological addition to ΛCDM that is able to resolve the Hubble tension [24], can emerge from first principles within a particle theory through thermal friction. This chapter is heavily based on [25], which I have written with coauthor Tanvi Karwal.

The value for the local expansion rate today H_0 is underpredicted by a ΛCDM model fit to the CMB by $> 4\sigma$. A new component added to ΛCDM that behaves like a cosmological constant at early times and then dilutes away as radiation or faster can resolve this tension [24,26]. In chapter 3, I show that a rolling axion coupled to a non-Abelian gauge group exhibits the behavior of such an extra component at the background level and can present a natural particle-physics model solution to the Hubble tension. Through thermal friction this model converts vacuum energy into a radiation component. Thus the requirements of the phenomenological solution are built in automatically, making it robust to a wide class of different potentials for the rolling field. In chapter 3, I make comparisons between this

particle model and the phenomenological solution, and determine that CMB observables sensitive only to the background evolution of the Universe are expected to be similar in both cases, strengthening the case for this model to provide a viable solution to the Hubble tension. Further evaluating the viability of this model requires investigating how the perturbations arising from the thermal friction in this model affect precision observables in the CMB. This is an exciting future prospect beyond the scope of this thesis.

Lastly in chapter 4, I am investigating cosmological probes of UV-extensions to the Standard model in the light of anomalous high-energy neutrino data at the IceCube detector. This chapter is based on [27] which I wrote with coauthors Melissa D. Diamond and David E. Kaplan.

The IceCube detector, a neutrino detector located in the Antarctic ice layer, has sensitivity to neutrinos from 10 - 10^{10} GeV [28]. The measured neutrino flux in the range between 30 TeV - 10 PeV has been significantly larger than estimates of the atmospheric background [29–32], suggesting an alternative source with a significance of at least 7 sigma [33]. No statistically significant correlation has been found between the detected neutrino directions and known astrophysical sources, thus suggesting the existence of an extra-galactic isotropic flux. In this work I consider long-lived heavy relics as a possible source for this extra-galactic isotropic flux with a focus on lifetimes that are shorter than the age of the universe. Exploring direct decays from the heavy relic to neutrinos, I consider two minimal particle models, their observational signatures in light of the IceCube anomaly, and the cosmological constraints on those signatures from secondary probes including BBN, the CMB and isotropic γ-ray detection.

Due to focusing on lifetimes shorter than the age of the universe, heavy relics with masses larger than 10 PeV are able to source the detected neutrino flux due to red-shifting. At those extremely high energies there are large electroweak corrections to the simple two body decay of the heavy relic to neutrinos, as higher multiplicity final states are no longer kinematically suppressed. In order to include those electroweak corrections, I developed a Monte Carlo simulation that incorporates the impact of electroweak showers to the neutrino spectra from the decaying ultra massive relic particle. By doing so, I was able to perform a detailed analysis of our signature beyond the scope of a mere toy-model, and apply the resulting insight to tighten the cosmological constraints as well as improve the comparison

of our theoretical predictions to the measured neutrino flux. I found that that there are two lifetime windows, one from $7*10^{10}$ s - 10^{12} s, and another one from $5*10^{14}$ s - $8*10^{1}6$ s, which are viable to source the excess flux without being ruled out by other cosmological probes. Further, I concluded that while a heavy decaying relic can account for the high-energy excess events (> 300 TeV), even including electroweak corrections which enhance the lower tail of the spectra, it cannot explain the low (50 TeV - 250 TeV) and high-energy excess at the same time. I also found that the decaying relic necessary to produce enough neutrino flux only needs to constitute a negligible sub-fraction of the total dark matter abundance in the universe.

There are many more interesting applications of minimal thermal friction as well as other novel extensions to the Standard model in cosmology, which lie beyond the scope of this thesis. The research presented in this thesis is part of my ongoing effort to explore the connection of novel particle physics models in a cosmological model building context, in the pursuit of contributing towards a complete fundamental theory.

"Simplicity is the keynote
of all true elegance."

— Coco Chanel

Chapter 2

Minimal Warm Inflation

The idea of an early period of cosmic inflation is a simple way to explain the near homogeneity and isotropy of the universe. Many of the simplest single-field models are already constrained by measurements of the scalar to tensor ratio r [34–36]. Warm inflation offers an interesting alternative [37–40] (for review, see [41]). It turns out to be possible to have a concurrent quasi-thermal radiation bath if energy is extracted from the rolling scalar field via friction. The benefits of warm inflation include automatic reheating at the end of inflation when the thermal bath begins to dominate over the vacuum energy and suppressing contributions to the scalar-tensor ratio r [40, 42]. It further enhances non-gaussianities and predicts a unique shape for the bispectrum, which is a 'smoking gun' for warm inflation, making it distinguishable from all other inflationary models [43]. Despite these benefits, in practice it has been challenging to embed warm inflation consistently within a microphysical theory due to large thermal backreactions on the inflaton potential [44], although progress has been made over the last twenty five years [40, 45–47].

In this chapter, we show that giving the inflaton an axion-like coupling naturally leads to warm inflation. This generates a thermal bath self-consistently without significant backreaction on the inflaton potential. The coupling can produce a simple theory of warm inflation consistent with all experimental data. We call this Minimal Warm Inflation.

Non-Abelian axion-like couplings in warm inflation have been considered before [48,49], without the explicit temperature dependence of the friction coefficient. Here, we use recent results of the sphaleron rate in classical lattice gauge theory, which predicts a dependence $\Upsilon \sim \alpha^5 \frac{T^3}{f^2}$ [50]. The temperature dependence greatly impacts predictions of cosmological observables [51] such as non-gaussianities, curvature power spectrum and spectral index, and thus needs to be included.

A different class of dissipative inflationary models with axion-like couplings exist that exploit rapid gauge field production through tachyonic instabilities [52,53]. Thermalization in these models is non-trivial but can happen, leading to an alternative setup of warm inflation [54,55]. In these works it has already been pointed out that the shift-symmetry of the axion can avoid thermal back-reactions.

This chapter is layed out as follows: in Section 2.1, we review the general properties of inflation when it is coupled to a thermal bath and point out that warm inflation is an attractor solution. In Section 2.2, we describe the specific case of a rolling field with an axion-like coupling to non-Abelian gauge fields and use the predicted temperature dependence to compute the power spectrum's tilt. In Section 2.3, we present a specific example of a potential, that of hybrid inflation, which matches cosmological data when the axion-like coupling is included. We present our conclusions in Section 2.4. We use Appendix 2.5 to describe the part of parameter space where thermal friction is sub-dominant (so-called weak warm inflation), which could in principle allow other potentials to reproduce the data, but in a regime where the calculations of the power spectrum from thermal fluctuations have not been done explicitly.

2.1 Background on Warm Inflation

We now give a terse summary of warm inflation (in the strong regime) including our definitions of the slow-roll parameters and a derivation of the power spectrum.

2.1.1 Framework of Warm Inflation

We will now show that it is possible to have a quasi-steady state cosmological solution with approximately constant vacuum energy and a non-negligible thermal bath with ap-

proximately constant temperature. We begin by considering the equation of motion of the inflaton in the presence of a temperature-dependent friction Υ. We define the dimensionless parameter $Q \equiv \frac{\Upsilon}{3H}$, such that:

$$\ddot{\phi} + 3H\left(1+Q\right)\dot{\phi} + V'(\phi) = 0 \tag{2.1}$$

which, together with the Friedman equation, governs the inflationary dynamics:

$$H^2 = \frac{1}{3M_{\rm Pl}^2}\left(V(\phi) + \frac{1}{2}\dot{\phi}^2 + \rho_R\right) \tag{2.2}$$

Here dots denote derivatives with respect to time ($\dot{\phi} = \frac{d\phi}{dt}$) and primes denote derivatives with respect to ϕ ($V'(\phi) = \frac{dV}{d\phi}$). During inflation the potential energy $V(\phi)$ dominates over both the kinetic energy $\frac{1}{2}\dot{\phi}^2$ and the radiation energy density ρ_R. We will see that ρ_R does not decrease during slow-roll and the end of inflation can occur when $V \sim \rho_R$. A small slow-roll parameter ϵ_H ensures that the evolution of the Hubble parameter is slow with respect to time:

$$\epsilon_H \equiv -\frac{\dot{H}}{H^2} \tag{2.3}$$

In order for accelerated expansion to be sustained, we impose another small slow-roll parameter η_H, which we take to be:

$$\eta_H \equiv -\frac{\ddot{H}}{\dot{H}H} + \frac{\ddot{\phi}}{H\dot{\phi}} \tag{2.4}$$

Here we have defined η_H such that it is independent of $\dot{Q}$. In the slow-roll regime where $\epsilon_H, \eta_H \ll 1$ we have:

$$\dot{\phi} \approx -\frac{V'}{3H(1+Q)} \tag{2.5}$$

$$H^2 \approx \frac{1}{3M_{\rm Pl}^2}V \tag{2.6}$$

By differentiating equations (2.5) and (2.6) with respect to time we obtain the slow-roll parameters in terms of the potential $V(\phi)$. To be consistent with the warm-inflation literature, we define:

$$\epsilon_V \equiv \frac{M_{\rm Pl}^2}{2(1+Q)}\left(\frac{V'}{V}\right)^2 \simeq \epsilon_H \ll 1 \tag{2.7}$$

$$\eta_V \equiv \frac{M_{\rm Pl}^2}{(1+Q)}\frac{V''}{V} \simeq \eta_H + \epsilon_H \ll 1 \tag{2.8}$$

Compared to cold inflation we can see that the conditions for slow-roll are relaxed due to the additional friction which permits slow-roll on steeper potentials. Thus, an advantage of warm inflation is that ϕ does not have to travel as far in field space to get the same number of e-folds. When Q is small this is only a small suppression; however when Q is large this allows sub-Planckian field values for ϕ, while still achieving the minimally required number of e-folds, $N_{\rm CMB} \sim 60$:

$$N_{\rm CMB} = \int H dt = \int_{\phi_{\rm end}}^{\phi_{\rm CMB}} \frac{1}{M_{\rm Pl}^2}\frac{V}{V'}\left(1+Q(\phi)\right) d\phi \tag{2.9}$$

In equation (2.9) $\phi_{\rm CMB}$ denotes the field value of ϕ at the beginning of the observable e-folds in the cosmic microwave background (CMB). $\phi_{\rm end}$ denotes the field value of ϕ at the end of inflation when the universe transitions into being radiation dominated. The energy extracted from the rolling field due to the friction sources the radiation bath [56]:

$$\dot{\rho}_R + 4H\rho_R = \Upsilon(T)\dot{\phi}^2 \tag{2.10}$$

In the slow-roll regime where ϵ_V, $\eta_V \ll 1$, we can neglect $\dot{\rho}_R$ and we obtain:

$$4H\rho_R \approx \Upsilon(T)\dot{\phi}^2 \tag{2.11}$$

for the quasi steady-state system.

2.1.2 Predictions of Warm Inflation

Here we focus on predictions in the strong regime ($Q \gg 1$) of warm inflation with a friction $\Upsilon \propto T^3$, which is the relevant friciton for our minimal warm inflation model as described in more detail in Section 2.2. In this regime the thermal inflaton perturbations dominate over the usually considered quantum fluctuations, as outlined in detail in, for example, [57]. The temperature dependence of the friction further couples the evolution of the inflaton and radiation fluctuations. This effect gives rise to a 'growing mode' for the curvature power spectrum, which is absent for a temperature-independent friction coefficient

or in the weak regime. The curvature power spectrum in presence of the growing mode has been calculated in [57][1] for $Q \gg 1$:

$$\Delta_R^2 \approx \frac{\sqrt{3}}{4\pi^{\frac{3}{2}}} \frac{H^3 T}{\dot{\phi}^2} \left(\frac{Q}{Q_3}\right)^9 Q^{\frac{1}{2}} \tag{2.12}$$

Here $Q_3 \approx 7.3$ and is fixed by matching the boundary conditions for the solution of the inflaton perturbations in different regimes.[2]

Assuming temperatures well below the Planck scale the tensor perturbations are not affected and remain the same as the prediction for cold inflation [59]:

$$\Delta_h^2 = \frac{2}{\pi^2} \frac{H^2}{M_{\rm Pl}^2} \tag{2.13}$$

The scalar to tensor ratio r based on equation (2.12) and (2.13) is then given by:

$$r \approx \frac{1}{\sqrt{3\pi}} \frac{16\epsilon_V}{Q^{\frac{3}{2}}} \frac{H}{T} \left(\frac{Q_3}{Q}\right)^9 \tag{2.14}$$

Equation (2.14) shows that r is heavily suppressed as: $\frac{H}{T} < 1$, $\epsilon_V \ll 1$, $Q \gg 1$ and $Q \gg Q_3$. This is in agreement with observational constraints as tensor modes have not been detected, yet. Contrarily, the detection of sizeable tensor modes in the future would rule out our model in the strong regime ($Q \gg 1$).

Sizeable non-gaussianities are the most distinct prediction of our minimal model of warm inflation since the total size of $f_{\rm NL}^{\rm warm}$ does not depend on slow-roll parameters. The strong regime of warm inflation $Q \gg 1$ has a unique dominant bispectrum shape [43, 60], which has been classified and constrained as 'WarmS' by the Planck 2015 results [61]. However, the Q-dependent result of $f_{\rm NL}^{\rm warm}$ [62] used in the Planck 2015 results to derive constraints on Q is only valid in the absence of a temperature-dependent friction coefficient and further suffers from a sign error as was pointed out by the authors of [62] in subsequent

[1] A different calculation from [58] suggests a scaling of $Q^{\frac{16}{2}}$ instead of $Q^{\frac{19}{2}}$. We thank Gauraw Gosmani for pointing this out. We do not take a position on this discrepancy, but note the impact on the results derived in this chapter is negligible.

[2] Approximation (2.12) is most accurate when $Q \gg Q_3$. Reference [57] also provides numerical results which approximate the spectrum down to $Q = 100$. Using the more accurate numerical results makes an negligible impact on the phenomenology discussed in this chapter. Thus, for easier readability we use the analytical approximation in equation (2.12).

work [60]. Considering the temperature dependence of the friction term of our 'minimal warm inflation model' gives a Q-independent prediction [43]:

$$f_{\rm NL}^{\rm warm} \approx 5 \tag{2.15}$$

This $f_{\rm NL}^{\rm warm}$ can be decomposed into contributions from different bispectral template shapes where $f_{\rm NL}^{\rm warmS} \approx 3.5$, $f_{\rm NL}^{\rm local} \approx 0.5$ and $f_{\rm NL}^{\rm equi} \approx 1$ [43]. Since the shape correlations between the 'WarmS' (equilateral) bispectral shape and the local bispectral shape is 0.27 (0.46) [63], the expected net contribution to the most constrained bispectral shape is $f_{\rm NL}^{\rm local} \approx 1.5$. The current most up to date constraints from Planck data are $f_{\rm NL}^{\rm local} = 0.8 \pm 5$ [61], which is insufficient for making conclusions about the viability of our model. While the not yet published Planck 2018 analysis may improve these bounds slightly, ideally an improvement of about a factor of ~ 10 in precision is needed to first discover sizeable non-gaussianities and second determine the bispectral shape. CMB Stage-4 [64] in accordance with upcoming optical, infrared and radio surveys conducted by new experiments such as Euclid [65], SPHEREx [66], and the SKA telescope [67] respectively report possible improvements over the current errorbars by up to a factor of $10 - 20$ [68, 69]. Euclid (SPHEREx) is planned to be launched before 2022 (2023) whereas the construction of the first SKA telescope (SKA1) is anticipated to start at the end of 2019. If the obtained experimental data will be able to match the precision level of the forecasts we will be able to conclusively detect the level of local non-gaussianity predicted by this model, which in a subsequent analysis could potentially be distinctively attributed to warm inflation due to its unique bispectral shape [43].

2.1.3 Initial Conditions for Warm Inflation

In this subsection we show that we do not have to start with a thermal bath to achieve warm inflation. In fact, for an inflaton that couples to light degrees of freedom with a wide range of couplings, a thermal bath will be automatically generated rapidly even starting from standard Hubble fluctuations.

If the universe starts with a low temperature it will start to heat up from the thermal friction which removes kinetic energy from the inflaton and dumps it into the thermal bath. It will tend towards the equilibrium temperature that comes from solving eqn. (2.11), but

we want to make sure this rate is fast enough that the equilibrium temperature is reached in a short time. To determine the time, we define constants A and B so that the radiation density $\rho_R = AT^4$ and the friction rate is $\Upsilon(T) = BT^p$ where we will assume the power $p < 4$ (which is the case for axion thermal friction as we will see below). We can see from eqn. (2.10) that if we start with a very low temperature then the Hubble term can be neglected and the evolution of the temperature is given by

$$\dot{\rho}_R \approx \Upsilon(T)\dot{\phi}^2 \tag{2.16}$$

Then eqn. (2.16) gives

$$T^{3-p}\,\frac{dT}{dt} = \frac{B\dot{\phi}^2}{4A} \tag{2.17}$$

we want to know that the equilibrium temperature can be reached quickly. For this it will be enough to find an upper bound on the time required $t_{\rm eq}$ to reach equilibrium. The temperature grows faster the larger $\dot{\phi}^2$. And note that initially at low temperatures the friction $\Upsilon(T)$ is lower than in equilibrium so the kinetic energy $\dot{\phi}^2$ will be larger (we assume here that the field ϕ has had time to come near its terminal velocity, but this takes at most a few e-folds). So to find an upper bound on $t_{\rm eq}$ it is conservative to assume $\dot{\phi}^2$ is fixed at its equilibrium value $\dot{\phi}^2_{\rm eq}$. Then we can solve eqn. (2.17) to find

$$T_{\rm eq}^{4-n} - T_i^{4-n} > (4-n)\frac{B\dot{\phi}^2_{\rm eq}}{4A}\,t_{\rm eq} \tag{2.18}$$

where T_i is the initial temperature. Note that the time it takes to heat up to the equilibrium temperature is essentially independent of the initial temperature (so long as it is relatively small). This surprising fact means we can start with any initial temperature (even quantum fluctuations of the fields would do it) and it will reach the equilibrium temperature in this same time.

In equilibrium we can solve eqn. (2.11) to find

$$HT_{\rm eq}^{4-n} = \frac{B\dot{\phi}^2_{\rm eq}}{4A} \tag{2.19}$$

Putting this into eqn. (2.18) we find that the time required to reach equilibrium is at most

$$t_{\rm eq} < \frac{1}{4-n}\frac{1}{H} \tag{2.20}$$

So it takes less than one Hubble time to reach the equilibrium temperature for warm inflation, no matter how low the initial temperature was (even including zero initial temperature since there are always quantum mechanical fluctuations).

Note that if we start with an initial temperature in the universe which is significantly above the equilibrium temperature $T_{\rm eq}$ then the temperature will drop through the normal redshifting (the Hubble term in equation (2.10)). This is not as fast as the rate we just found for the temperature approaching equilibrium from below which had the interesting behavior that it was independent of the initial temperature. In the case of the temperature dropping towards equilibrium, it does take more than one Hubble time, but since the reshifting is exponential it only takes $\sim \ln\left(\frac{T_i}{T_{\rm eq}}\right)$ e-folds of inflation before the temperature has dropped to equilibrium.

We have seen that our warm inflation is an attractor solution. Given a potential for an inflaton, and some terms that allow the inflaton to interact with other light degrees of freedom, a thermal bath will be generated very rapidly at the start of inflation. So it is generic to be in warm inflation instead of cold inflation, as long as the light degrees of freedom are lighter than the equilibrium temperature. Of course if the equilibrium temperature is low enough that $T_{\rm eq} < H$ then having this thermal bath is meaningless and we are actually in cold inflation.

2.1.4 The Problems of Warm Inflation

It is challenging to build a microphysical model that supports warm inflaton because the friction Υ is usually accompanied by a large thermal back-reaction onto the inflaton potential, that spoils the flatness of the potential and does not support enough e-folds. When the friction arises from perturbative interactions directly between the scalar field and light fields, the mass of the scalar fields obtains a finite temperature contributions which scales with the temperature:

$$\delta m_\phi^2 \propto T^2 \tag{2.21}$$

This correction is dominant to the friction which scales with temperature fluctuations $\Upsilon \propto \delta T$. It is possible to protect the mass of the inflaton from thermal contributions by imposing symmetries; however this generically also turns off the friction. Thus, it appears challenging to produce a large friction without unwanted mass corrections or fine-tuned cancellations.

2.2 Warm Inflation with an Axion

We find a minimal warm inflation model in which the inflaton ϕ is an axion coupling to a pure Yang-Mills gauge group:

$$\mathcal{L}_{\rm int} = \frac{\alpha}{16\pi}\frac{\phi}{f}\tilde{G}^{\mu\nu}_a G^a_{\mu\nu} \tag{2.22}$$

Here $G^a_{\mu\nu}$ ($\tilde{G}^a_{\mu\nu} = \epsilon^{\mu\nu\alpha\beta}G^a_{\alpha\beta}$) is the field strength of an arbitrary Yang-Mills group and $\alpha \equiv \frac{g^2_{\rm YM}}{4\pi}$, and $g_{\rm YM}$ is the gauge coupling. There is no perturbative back-reaction that scales with the temperature because the axion is protected by its shift symmetry[3]. The back-reaction due to non-perturbative effects is just the usual axion mass, which at zero temperature scales as $\propto \frac{T_c^4}{f^2}$ and at high temperatures ($T \gg T_c$) this small quantity becomes even further surpessed as instanton methods [70] estimate a power-law decrease with $m_a^2 \propto T^{-X}$, with $X \sim 7$ for pure Yang-Mills SU(3) [71], which is in agreement with lattice calculations. This is why the back-reaction in our model is negligible.

However, at high temperatures classical transitions between vacua with different topological charge are no longer suppressed, which give rise to topological charge fluctuations. Thus, the fluctuations responsible for the friction experienced by ϕ are not inherently thermal; they are topological. However, the topological fluctuations still increase with temperature as higher temperatures enhance the transition rate, also known as the sphaleron rate $\Gamma_{\rm sphal} = \lim_{V,t\to\infty}\frac{\langle Q^2\rangle}{Vt}$ [72]. The friction arising from the interaction in (3.1) can be determined by the sphaleron rate $\Gamma_{\rm sphal}$ in the limit of the inflaton mass being smaller than $\sim \alpha^2 T$ [73]:

$$\Upsilon(T) = \frac{\Gamma_{\rm sphal}(T)}{2f^2T} \tag{2.23}$$

The sphaleron rate has been measured within classical lattice gauge theory for pure SU(2)

[3]We softly break this symmetry by giving the inflaton a UV-potential. We have checked that the back-reaction from this breaking term is negligible.

and SU(3) theories and indicates a scaling of $\Gamma_{\text{sphal}} \sim \alpha^5 T^4$ [50,73]. The friction coefficient Υ then scales roughly as T^3 [50]:

$$\Upsilon(T) = \kappa(\alpha, N_c, N_f)\alpha^5 \frac{T^3}{f^2} \tag{2.24}$$

where T is the temperature of the thermal bath of the Yang-Mills group and this formula only applies when that group is in thermal equilibrium[4]. κ is an O(100) number which has a weak logarithmic dependence on α and whose exact value depends on the number of colors N_c and flavors N_f of the group [50]. The estimate of the friction coefficient in terms of the sphaleron rate breaks down in the weak regime of warm inflation ($Q \lesssim 1$) due to the limit $m_\phi \ll \alpha^2 T$ becoming oversaturated. While the mechanism itself should also work for the weak regime, we focus on the strong regime in this chapter since we know the exact friction in this regime. Thermalization of the inflaton occurs in this regime if the gauge boson-inflaton scattering rate, $\Gamma_{g\phi} \approx \alpha^3 \frac{T^3}{32\pi f^2}$ [74,75], is much larger than the Hubble rate. This gives the condition $\frac{3Q}{32\pi\kappa\alpha^2} \gg 1$, which is always satisfied in the strong regime of our model, where we consider $Q > 100$ and $\alpha < 0.1$.

We give the inflaton a UV-potential $V(\phi)$ (in addition to the IR potential it would get from the confining group). We cannot use the IR potential because, in order to have a thermal bath of gauge bosons, we must have the temperature above the confinement scale. At such temperatures the IR potential is rapidly suppressed and we have checked that it is not possible to use that potential for inflation. So inflation occurs as the inflaton rolls down its UV potential V and its equation of motion is given by:

$$\ddot{\phi} + (3H + \Upsilon)\,\dot{\phi} + V'(\phi) = 0 \tag{2.25}$$

Based on the curvature power spectrum in equation (2.12) we derive the spectral index:

$$n_s - 1 = \frac{d\ln\Delta^2_{\mathcal{R}}}{dN} \tag{2.26}$$

$$\frac{d\ln\Delta^2_{\mathcal{R}}}{dN} = \left(\frac{5}{2} - 9\right)\frac{d\ln H}{dN} - 2\frac{d\ln\dot{\phi}}{dN} + \left(\frac{1}{2} + 9\right)\frac{d\ln\Upsilon}{dN} + \frac{d\ln T}{dN} \tag{2.27}$$

[4]We are ignoring the weak T-dependence in the running of α as T remains nearly constant during the period of inflation, and thus α can be treated as a fixed parameter of the model.

Using $Hdt = dN$ we rewrite the derivatives in equation (2.27) in terms of the slow-roll parameters [76]:

$$\frac{d\ln H}{dN} = -\epsilon_V \tag{2.28}$$

$$\frac{d\ln\dot{\phi}}{dN} = \epsilon_V - \eta_V - \frac{Q}{1+Q}\frac{d\ln Q}{dN} \tag{2.29}$$

$$\frac{d\ln Q}{dN} = \epsilon_V + 3\frac{d\ln T}{dN} \tag{2.30}$$

We use equation (2.11) to express the temperature as a function of time resulting in:

$$\lim_{Q\gg 1}\frac{d\ln T}{dN} = \frac{1}{7}\left(\epsilon_V - 2\eta_V\right) \tag{2.31}$$

$$\frac{d\ln\Upsilon}{dN} = 3\frac{d\ln T}{dN} \tag{2.32}$$

Plugging in (2.28), (2.29), (2.31) and (2.32) into (2.27) we find the spectral index in leading order in ϵ_V and η_V in the strong regime of warm inflation:

$$n_s - 1 = \frac{3}{7}\left(27\epsilon_V - 19\eta_V\right) \tag{2.33}$$

Compared to the spectral tilt obtained from the standard cold inflation power spectrum the sign of ϵ_V and η_V is inverted for the strong regime of warm inflation. This conveys interesting constraints on possible potential shapes for warm inflation that are in agreement with the observed red tilt ($n_s - 1 < 0$), as η_V has to be larger than ϵ_V.

2.3 An Example: Hybrid Warm Inflation

2.3.1 Inflation

In the strong regime of warm inflation the expression for the spectral tilt in (2.33) only reproduces the experimentally observed red tilt when $\epsilon_V < \eta_V$. For a single scalar field model this requires a fine-tuned level of convexity of the potential $V \propto \phi^n$ with $n \gtrsim 4$. Similarly, the lowest order cosine-like potential that is able to reproduce the observables requires $V \propto (1 + \cos\frac{\phi}{f_\phi})^n$ with $n \geq 3$. In particular, a single cosine does not fit the observations. As an example, Figure 2.1 shows how $V \propto \phi^5$ can reproduce the observed spectral index in single field inflation. However, we do not think that these potentials are

compelling candidates, as they do not easily emerge from a UV-completion without extreme fine-tuning.

In contrast, the simplest setup for hybrid inflation [77] with a slow-roll potential $V \sim V_0 + \frac{1}{2}m^2\phi^2$, usually ruled out due to predicting a blue tilted spectrum, works well with warm inflation in the strong regime. As an example, we explore the inflationary dynamics for warm inflation in a hybrid setup in this section, where the inflaton field ϕ couples to a pure SU(3) gauge group, as described in Section 2.2.

The effective potential in hybrid inflation has two fields, one that acts as the inflaton ϕ and another the waterfall field σ that stays constant during the inflationary period:

$$V(\phi,\sigma) = \frac{1}{4\lambda}\left(M^2 - \lambda\sigma^2\right)^2 + \frac{1}{2}m^2\phi^2 + \frac{1}{2}g^2\phi^2\sigma^2 \tag{2.34}$$

The squared mass of the waterfall field σ is equal to $-M^2 + g^2\phi^2$. While $\phi > \frac{M}{g}$, σ only has one minimum at $\sigma = 0$. Inflation ends when ϕ reaches this threshold, which induces a first order phase-transition causing σ to roll down to its minimum at $\sigma(\phi) = \frac{M_\sigma(\phi)}{\sqrt{\lambda}}$, with $M_\sigma(0) = M$. After the phase transition, ϕ rolls to the minimum of its effective potential much faster than a Hubble time as long as:

$$M^3 \ll \frac{\sqrt{\lambda}gmM_{\rm Pl}^2}{Q} \tag{2.35}$$

The waterfall field σ rapidly starts oscillating after the phase transition as long as $M_\sigma(\phi) \gg H$. Under those conditions, inflation ends almost instantaneously.

We can then describe the effective potential for the inflaton field ϕ during the time of inflation as:

$$V_{\rm eff}(\phi) = \frac{M^4}{\lambda} + \frac{1}{2}m^2\phi^2 \tag{2.36}$$

In the allowed parameter space outlined below, σ's mass is larger than the temperature during inflation. Thus, σ does not thermalize and corrections to the thermal mass of ϕ turn out to be negligible. The observable amounts of e-folds occur as ϕ is approaching its critical value $\phi_c \equiv \frac{M}{g}$, which induces the phase transition. During this stage the constant term $\frac{M^4}{\lambda} \gg \frac{1}{2}m^2\phi_c^2$ drives the expansion, effectively suppressing ϵ_V. While ϕ is approaching its critical value it is sourcing a thermal bath via friction Υ. The spectral index (2.33) then

simplifies to:

$$n_s - 1 \approx -\frac{57}{7}\eta_V \tag{2.37}$$

with:

$$\eta_V = \frac{4\lambda m^2 M_{\rm Pl}^2}{QM^4} \tag{2.38}$$

The spectral tilt fixes the following linear combination of parameters:

$$\frac{4\lambda m^2 M_{\rm Pl}^2}{QM^4} \approx -\frac{7}{57}(n_s - 1) \tag{2.39}$$

Assuming inequality Eqn. (2.35) is satisfied we can approximate $\phi_c \approx \phi_{\rm end}$. Rewriting equation (2.9) in the strong regime with $Q \gg 1$, and $\phi_{\rm CMB} = (1+\Delta)\phi_c$, with $\Delta < 1$, we find:

$$N_{\rm CMB} = \int_{\frac{M}{g}}^{\frac{M}{g}(1+\Delta)} \frac{1}{M_{\rm Pl}^2}\frac{V}{V'}Q(\phi)d\phi \tag{2.40}$$

Using equation (2.5), (2.6), and (2.11) we express T and Q in terms of ϕ during slow-roll, where $\rho_R = \frac{\pi^2}{30}g_* T^4 \equiv \tilde{g}_* T^4$, with g_* denoting the relativistic degrees of freedom:

$$T(\phi) \approx \left(\frac{f^2}{\kappa\alpha^5}\frac{\sqrt{3}M_{\rm Pl}V'(\phi)^2}{2\tilde{g_*}\sqrt{V(\phi)}}\right)^{\frac{1}{7}} \tag{2.41}$$

$$Q(\phi) \approx \left(\left(\frac{\kappa\alpha^5}{f^2}\right)^4 \frac{M_{\rm Pl}^{10}V(\phi)'^6}{576\tilde{g_*}V(\phi)^5}\right)^{\frac{1}{7}} \tag{2.42}$$

Using equations (2.36) and (2.42) in equation (2.40) and assuming $\frac{M}{g} \ll M_{\rm Pl}$, we obtain:

$$N_{\rm CMB} \approx \frac{\Delta}{\eta_V} \tag{2.43}$$

The number of observable e-folds, $N_{\rm CMB} \approx 60$, then only impacts the transversed field range Δ:

$$\Delta \approx -\frac{7}{57}(n_s - 1)N_{\rm CMB} \tag{2.44}$$

Equation (2.44) determines Δ in terms of measured observables. Equation (2.39) determines another linear combination of $\lambda, g, M, m, f, \Delta$ in terms of observables. The measured

amplitude of the curvature power spectrum fixes one additional linear combination:

$$\Delta_R^2(k) = A_s(k_*)\left(\frac{k}{k_*}\right)^{n_s(k_*)} \tag{2.45}$$

with $A_s(\phi_{CMB}) \approx 2\times10^{-9}$ as measured by Planck at the pivot scale $k_* = 0.05\text{Mpc}^{-1}$ [13]. Rewriting equation (2.12) we find:

$$A_s\left(\phi_{\text{CMB}}\right) \approx 8\times10^{-41}\left(\frac{\kappa\alpha^5}{f^2}\right)^{18}\left(\frac{\sqrt{|n_s-1|}^{81} m^{21}\phi_{\text{CMB}}^{51}}{\sqrt{\tilde{g_*}}^{55}}\right)^{\frac{1}{2}} \tag{2.46}$$

where $\phi_{\text{CMB}} = \frac{M}{g}(1+\Delta) \approx \frac{M}{g}$.

We have used the spectral index n_s, amount of observable e-folds N_{CMB}, and the amplitude of the power spectrum A_s, to constrain three of the parameters of the underlying model. The friction ratio Q depends on the ratio of the coupling f to the field value of the inflaton $\sim \frac{M}{g}$ during inflation as:

$$Q \approx 150\left(\frac{\Delta_R^2}{2\times10^{-9}}\right)^{\frac{2}{21}}\left(\frac{|n_s-1|}{0.035}\right)^{\frac{4}{7}}\left(\frac{g_*}{17}\right)^{-\frac{4}{21}}\left(\frac{\kappa\alpha^5}{10^{-3}}\right)^{\frac{2}{7}}\left(\frac{\frac{gf}{M}}{10^{-8}}\right)^{-\frac{4}{7}} \tag{2.47}$$

Where we use a pure SU(3) with $g_* = 17$ (two polarizations per eight gauge bosons plus one for the axion) and gauge coupling $\alpha = 0.1$ as our default values. The only tunable parameter beyond these is $\frac{gf}{M}$ which has to be $\lesssim 10^{-8}$ to place us in the strong regime ($Q \gg 1$), thus setting the upper bound $f \ll 10^{-8}(M/g)$ for these gauge group parameters. The typical Hubble scales and mass parameters in our model are thus:

$$H \approx 10^{-17}\left(\frac{\Delta_R^2}{2\times10^{-9}}\right)^{\frac{1}{21}}\left(\frac{|n_s-1|}{0.035}\right)^{-\frac{19}{7}}\left(\frac{g_*}{17}\right)^{\frac{59}{42}}\left(\frac{\kappa\alpha^5}{10^{-3}}\right)^{-\frac{13}{7}}\left(\frac{\frac{gf}{M}}{10^{-8}}\right)^{\frac{19}{7}}\frac{M}{g} \tag{2.48}$$

$$m \approx 10^{-16}\left(\frac{\Delta_R^2}{2\times10^{-9}}\right)^{\frac{2}{21}}\left(\frac{|n_s-1|}{0.035}\right)^{-\frac{12}{7}}\left(\frac{g_*}{17}\right)^{\frac{55}{42}}\left(\frac{\kappa\alpha^5}{10^{-3}}\right)^{-\frac{12}{7}}\left(\frac{\frac{gf}{M}}{10^{-8}}\right)^{\frac{24}{7}}\frac{M}{g} \tag{2.49}$$

Note that m can be larger than H, without violating slow-roll due to the dominant friction

coming from $\Upsilon \gg H$. Typical temperatures during expansion are given by:

$$T \approx 5 \times 10^{-10} \left(\frac{\Delta_R^2}{2 \times 10^{-9}}\right)^{\frac{1}{21}} \left(\frac{|n_s - 1|}{0.035}\right)^{-\frac{12}{7}} \left(\frac{g_*}{17}\right)^{\frac{17}{42}} \left(\frac{\kappa\alpha^5}{10^{-3}}\right)^{-\frac{6}{7}} \left(\frac{\frac{gf}{M}}{10^{-8}}\right)^{\frac{12}{7}} \frac{M}{g} \tag{2.50}$$

Demanding that condition (2.35) is satisfied such that inflaton quickly rolls to its minimum after the phase transition imposes an upper limit on $\frac{M}{g}$:

$$\frac{M}{g} \ll 3 \times 10^{-3} \left(\frac{\Delta_R^2}{2 \times 10^{-9}}\right)^{-\frac{1}{21}} \left(\frac{|n_s - 1|}{0.035}\right)^{\frac{3}{14}} \left(\frac{g_*}{17}\right)^{\frac{2}{21}} \left(\frac{\kappa\alpha^5}{10^{-3}}\right)^{-\frac{1}{7}} \left(\frac{\frac{gf}{M}}{10^{-8}}\right)^{\frac{2}{7}} M_{\rm Pl} \tag{2.51}$$

The above condition demands that the maximum allowed value for $\frac{M}{g}$ is roughly $10^{14}\,\text{GeV}$. This value sets an upper limit for the possible temperatures of $T < 5 \times 10^4\,\text{GeV}$ and Hubble scales of $H < 10^{-3}\,\text{GeV}$. The discussed observables degenerately depend on combinations of M, λ and g. Requiring the quantum corrections to our masses be naturally small also imposes constraints that break the degeneracy:

$$\frac{\lambda^2\Lambda^2}{16\pi^2} < M^2 \tag{2.52}$$

$$\frac{g^2\Lambda^2}{16\pi^2} < m^2 \tag{2.53}$$

where Λ is the cutoff of the theory. The couplings g and λ need to satisfy conditions (2.52) and (2.53). Additionally, the condition that the ϕ potential is negligible compared to the vacuum energy during inflation requires:

$$\frac{\lambda m^2}{g^2} \ll M^2 \tag{2.54}$$

Assuming a minimum value of the cutoff $\Lambda = 4\pi M$, saturating equation (2.53) and $\frac{M}{g} = 10^{14}\,\text{GeV}$, and satisfying (2.54) by two orders of magnitude, we get the following sample values for the couplings and mass parameters: $g = 10^{-8}$, $\lambda = 10^{-2}$, $M = 10^6\,\text{GeV}$, $m = 10^{-2}\,\text{GeV}$.

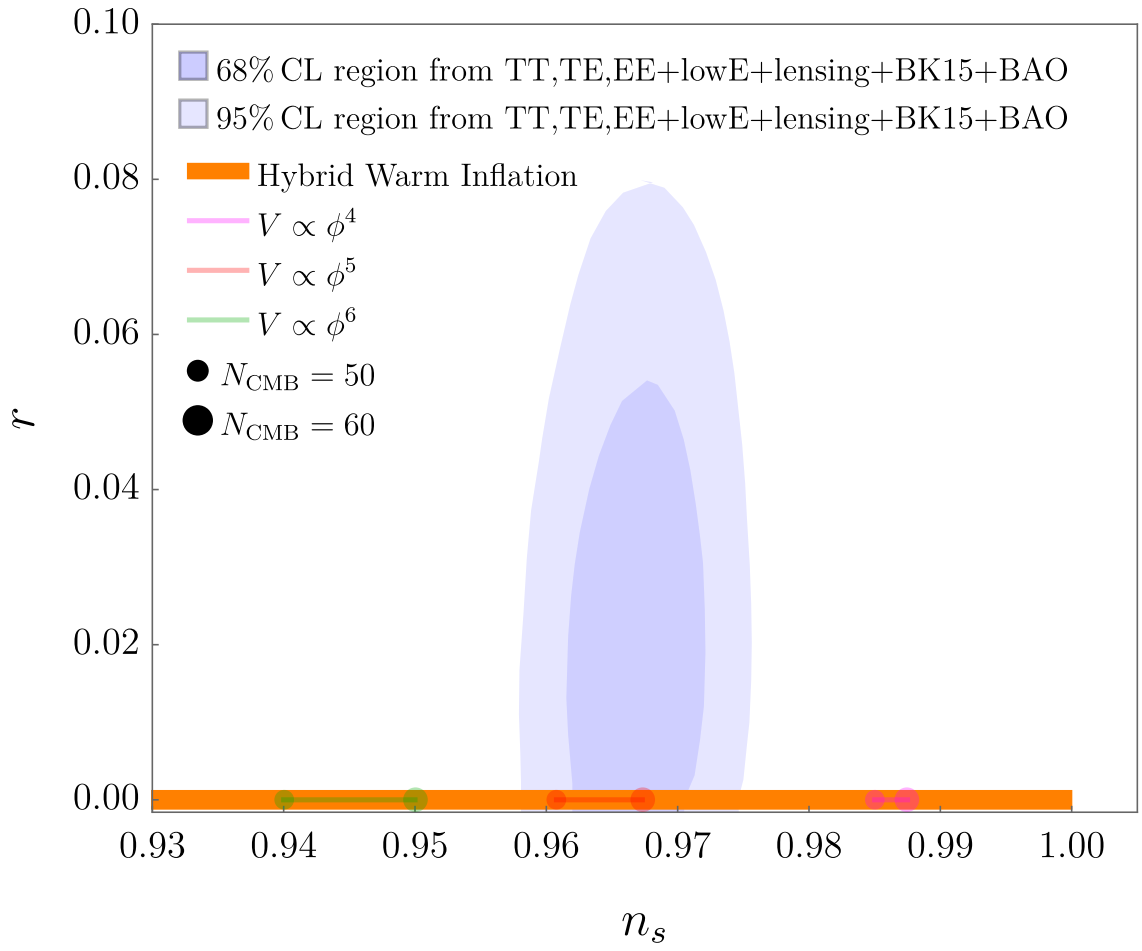

Figure 2.1: Comparison of the predicted spectral index n_s in the strong regime of minimal warm inflation, given different potentials. Hybrid warm inflation overlaps with the allowed region. Due to remaining free parameters in hybrid inflation it is able to reproduce various red-tilted values of n_s. In single field inflation $V \propto \phi^5$ lies in the allowed region in the r-n_s plane (although such a potential in general is not compelling as it requires extreme fine-tuning). All predictions for the tensor-to scalar ratio in the strong regime are $r \approx 0$ due to the heavy surpression of r for $Q \gg 1$. The shown allowed contour regions are the most stringent to date using Planck 2018 data as well as lensing, polarizations data from BICEP2/Keck Array BK15 and baryon acoustic oscillation (BAO).

2.3.2 Reheating

At reheating, we assume that we have an abundance of σ particles at some early time before big bang nucleosynthesis, which make up a dominant part of the energy density in the early universe. There are many possible ways in which σ can couple to the standard model and produce an early quark gluon plasma. Here we outline a simple example where we couple to standard model hypercharge:

$$\mathcal{L}_{\text{reheat}} = \frac{g'^2}{64\pi^2}\frac{\sigma}{f_B}\tilde{B}^{\mu\nu}B_{\mu\nu} \tag{2.55}$$

where g' denotes the standard model hypercharge gauge coupling. Typical values of the coupling between the waterfall and inflaton fields in our model (g) are quite small, which is why σ decays dominantly via operator (2.55), even for large values of f_B. We can estimate the decay rate into standard model particles by:

$$\Gamma_{\sigma\to\text{SMSM}} = \frac{g'^4 M^3}{16384\pi^5 f_B^2} \tag{2.56}$$

This rate needs to be large enough such that an abundance of σ particles has decayed into a quark gluon plasma before the universe cools down to big bang nucleosynthesis temperatures, where the earliest cosmological precision constraints exist. We estimate the Hubble rate as $H_{\text{BBN}} \approx \frac{\sqrt{\frac{g_*\pi^2}{30}}T_{\text{BBN}}^2}{\sqrt{3}M_{\text{Pl}}}$ and demanding that $\Gamma_{\sigma\to\text{SMSM}} > H_{\text{BBN}}$ we find that f_B can go all the way up to the GUT scale:

$$f_B < 10^{16}\,\text{GeV}\left(\frac{M}{10^6\,\text{GeV}}\right)^{\frac{3}{2}}\left(\frac{T_{\text{BBN}}}{10\,\text{MeV}}\right)^{-1} \tag{2.57}$$

At the end of section 2.3.1 we briefly discuss the upper limits of masses, temperatures and Hubble scales. Here we discuss the lower limits of our parameters. Since the waterfall field σ couples directly to the standard model there exist cooling bounds from supernovae as well as detection constraints from high-energy colliders. Avoiding these, we conservatively set $f_B > 1\,\text{TeV}$ and $M > 10\,\text{GeV}$ as the lower limits of our parameter space which fixes $m > 10^{-7}\,\text{GeV}$, $H > 10^{-8}\,\text{GeV}$ and $T > 0.5\,\text{GeV}$, where T is the temperature during slow-roll maintained by the pure Yang-Mills radiation. These parameters easily still satisfy the cosmological constraints that reheating happens efficiently before BBN. Summarizing our

available parameter space we find these:

$$10^{-8}\,\mathrm{GeV} < H < 10^{-3}\,\mathrm{GeV} \tag{2.58}$$

$$10^{-7}\,\mathrm{GeV} < m < 10^{-2}\,\mathrm{GeV} \tag{2.59}$$

$$10\,\mathrm{GeV} < M < 10^{6}\,\mathrm{GeV} \tag{2.60}$$

$$0.5\,\mathrm{GeV} < T < 5 \times 10^{4}\,\mathrm{GeV} \tag{2.61}$$

$$0.5\,\mathrm{GeV} < f < 5 \times 10^{6}\,\mathrm{GeV} \tag{2.62}$$

are the maximally allowed ranges for each parameter, though of course there are restrictions on the combination of the five parameters (e.g. the requirement of decay before BBN and the validity of the effective field theory). The question remains whether the inflaton coupling to a standard model gauge group itself (e.g. QCD) can give rise to a thermal bath sourcing friction during inflation. In that scenario, a quark gluon plasma is already present during the expansion of the universe and reheating becomes trivial. However, currently detailed calculations of the friction coefficient exist only for pure Yang-Mills theory. The presence of light fermions may non-trivially alter the parametric dependence[5], in which case a separate analysis is necessary to determine whether this compelling simplification is viable. We leave that analysis and the calculation of the friction in the presence of light fermions to future work.

2.4 Conclusions

If the inflaton has any non-gravitational coupling to other fields it will generically produce a background thermal bath during inflation. A natural choice is an axion-like (CP-odd) coupling which can generate significant thermal friction from non-perturbative effects for the inflaton without a corresponding backreaction on the inflaton potential, thus avoiding the problems with other warm inflation models. Once the inflaton has any such strong enough coupling, a thermal bath will necessarily be produced during inflation independent of initial conditions.

We have presented a complete model of warm inflation which correctly reproduces cos-

[5]This concern was pointed out to us by members of the theory group at the University of Maryland. We thank them and Guy Moore for extensive discussions on this topic.

mological data on initial density perturbations and predicts a negligible tensor-to-scalar ratio r and potentially measureable non-gaussianities. The model only requires the inflaton to have an axion-like coupling to a non-Abelian group, and we use known results for couplings to pure Yang-Mills. An even simpler model may be possible where the inflaton couples directly to the standard model (such as to QCD), but a full thermal field theory calculation of the friction in this case (specifically with light quarks) has not yet been done. We show, as an example, that the temperature dependence of the friction due to our coupling allows hybrid inflation to have a red-tilted spectrum (rather than blue-tilted as in cold inflation), and thus can easily fit the current data.

2.5 The Weak Regime

Due to the calculations of the friction coefficient breaking down in the weak regime we have focused on exploring the strong regime ($Q \gg 1$) in detail in this chapter. In this appendix we summarize the relevant dynamics in the weak regime. It turns out that the only viable models of warm inflation we could find in the weak regime require parameters which move the thermal friction beyond the regime of validity of the thermal field theory calculations which have been done. Thus in this section we will simply assume that the friction coefficient still scales as $\Upsilon \sim \kappa\alpha^5 \frac{T^3}{f^2}$, and discuss warm inflation in this case. But we will find that in fact we are ultimately pushed to a regime of parameters where this formula is not known to be valid. So it is in fact possible that a weak warm inflation model would work – even for a simple inflaton potential $m^2\phi^2$ – but we cannot know that from the thermal field theory calculations that have been done to date.

In the weak regime of warm inflation ($Q \ll 1$) the dominant friction in the inflaton's equation of motion is still due to the Hubble expansion rather than particle production friction. However, the presence of a thermal bath can still change the power spectrum and effectively surpress the scalar-to-tensor ratio. Unlike in the strong regime the temperature dependent friction coefficient does not give rise to a growing mode as the coupling between the radiation and the inflaton can be neglected. The curvature power spectrum and the scalar to tensor ratio in this regime can then be described by [38,78,79], where all quantities

are evaluated at horizon crossing:

$$\Delta_R^2 = \frac{1}{4\pi^2}\frac{H^4}{\dot{\phi}^2}\left(1+2n+2\pi Q\frac{T}{H}\right) \tag{2.63}$$

$$r = \frac{16\epsilon_V}{\left(1+2n+2\pi Q\frac{T}{H}\right)} \tag{2.64}$$

Here n denotes the distribution of inflaton particles. If interactions between the inflaton particles and the thermal bath are sufficiently fast for them to be thermalized then they approach a Bose-Einstein distribution, which at horizon crossing is given by $n_{\rm BE} = \left(e^{\frac{H}{T}}-1\right)^{-1}$. Whether thermalization is fast enough is model dependent. The interaction rate for the axion-inflaton with the gauge boson radiation, $\Gamma_{\phi g}$, can be roughly approximated as $\Gamma_{\phi g} \approx \alpha^3\frac{T^3}{32\pi f^2} = \frac{\Upsilon}{32\pi\kappa\alpha^2}$. The inflaton is thermalized ($\Gamma_{\phi g} > H$), when $\frac{3Q}{32\pi\kappa\alpha^2} > 1$, which is satisfied for $\alpha \lesssim 10^{-2}\sqrt{Q}$. Thus, whether thermalization occurs depends on the gauge coupling of the YM-group itself. For a temperature dependence of the friction $\Upsilon \propto T^3$, we can derive the spectral index in the weak regime using equations (2.28), (2.29), (2.32), (2.27) and:

$$\lim_{Q\ll 1}\frac{d\ln T}{dN} = (3\epsilon_V - 2\eta_V) \tag{2.65}$$

finding:

$$n_s - 1 = \frac{1}{1+2n+\frac{2\pi QT}{H}}(2\eta_V - 6\epsilon_V) + \frac{\frac{2\pi QT}{H}}{1+2n+\frac{2\pi QT}{H}}(8\epsilon_V - 6\eta_V) + \frac{2n}{1+2n+\frac{2\pi QT}{H}}(-2\epsilon_V) \tag{2.66}$$

If the inflaton is not thermalized and $\frac{2\pi QT}{H} \ll 1$ we recover the regular cold inflation result. The size of this parameter determines whether we are in a regime in which thermal fluctuations dominate over quantum effects. When quantum effects dominate the spectral index obtains a higher order correction, which is negligible. However, when thermal fluctuations dominate we again obtain a spectral index that can only be red-tilted for potentials where η_V dominate, again demanding a fine-tuning of single field potentials, similarly to the strong case. If the inflaton is fully thermalized the third term in equation (2.66) dominates as $n \sim \frac{T}{H}$ and $Q \ll 1$. However, for single field potentials the predicted spectral index n_s for about 50 to 60 e-folds lies outside of the two sigma region. There does exist a transition region where the inflaton is not fully thermalized for $n \sim \frac{2\pi QT}{H} < 1$, where the observed spectral tilt can be reproduced in the weak regime. However, in this transition region non-

gaussianity constraints become important [43]. For detailed non-gaussianity predictions in the weak regime in the presence of a friction that scales as $\Upsilon \propto T^3$, see [43].

The weak warm inflation formulas above have only been calculated in the regime where $Q \ll 1$ (for a temperature-dependent friction coefficient). Additionally, being conservative we are only certain we can trust the thermal field theory calculations when $\alpha^2 T > H$ and $\alpha^2 T > m$ (where m is the mass of the inflaton). Taking the combination of all these constraints on the validity of the calculations that have been done, we find no region of parameter space that can fit the observations (the values of n_s, r, number of e-folds and the size of the perturbations). So we are unable to make an observationally viable weak warm inflation model. However it is possible that if the calculations for warm inflation were extended to include a region of $Q \sim 1$ (for our temperature-dependent friction) one could find a viable inflation model. Or similarly it is possible that if the thermal field theory calculations were valid beyond $\alpha^2 T > H$ and $\alpha^2 T > m$ then one could find a viable weak warm inflation model. We leave this for future work.

"Logic will get you from A to B. Imagination will take you everywhere."

— Albert Einstein

Chapter 3

Thermal friction as a solution to the Hubble tension

The tremendously successful standard model of cosmology assumes a flat universe, cold dark matter (CDM) and cosmological-constant dark energy Λ. This ΛCDMmodel correctly describes numerous observables including the the complex structure of the cosmic microwave background (CMB) spectra [13, 23]. However, its predictions for the current rate H_0 of expansion of the Universe based on the CMB are discrepant with the most precise direct measurements in the local universe at $> 4\sigma$ [22, 80–82]. With no obvious systematic cause in sight [83–93], this worsening tension has inspired many theorists to postulate new physics beyond the ΛCDM model [22, 94–97]. However, few solutions exist [24, 26, 95, 98–100] that simultaneously resolve the Hubble tension while also providing a good fit to all observables.

One of the more successful solutions is the addition of an early dark energy (EDE) component [24,98,99,101], disjoint from the late-time dark energy. This component behaves like a cosmological constant at early times, then dilutes away as fast or faster than radiation at some critical redshift z_c, localizing its influence on cosmology around z_c. It increases the pre-recombination expansion rate, decreasing the size r_s of the sound horizon. The CMB inference of H_0 is based on r_s and its angular size θ_* on the surface of last scatter. Precise observations of θ_* combined with a ΛCDM-based deduction of r_s determine H_0

as $\theta_* \sim r_s H_0$. Hence, a theory that predicts a smaller r_s also infers a greater H_0 to preserve the precisely measured θ_*, alleviating the Hubble tension. It was proposed as a phenomenological solution, the dynamics of which could emerge from various particle-physics models [26, 98, 99, 102–104].

In this chapter, we present a dynamical particle-physics model that could solve the Hubble tension, which at the background level, mimics the evolution of early dark energy. This model, the "dissipative axion" (DA), is presented in Sec. 3.1. Although we leave the details of the perturbations of this model to future work, in Sec. 3.2, we argue why the background dynamics of this model are promising and indicate that the DA can form an extra dark energy component that resolves the Hubble tension. We conclude in Sec. 3.3, where we discuss the broader implications of this model and the way forward.

3.1 Model

We add a pure dark non-Abelian gauge group [SU(2)] and an axion ϕ to the Standard Model particle content. The dark gauge bosons interact with ϕ via a CP-odd coupling,

$$\mathcal{L}_{\rm int} = \frac{\alpha}{16\pi}\frac{\phi}{f}\tilde{F}^{\mu\nu}_{a}F^{a}_{\mu\nu}\,, \tag{3.1}$$

where $F^a_{\mu\nu}$ ($\tilde{F}^a_{\mu\nu} = \epsilon^{\mu\nu\alpha\beta}F^a_{\alpha\beta}$) is the field strength of the dark gauge bosons and $\alpha = \frac{g^2}{4\pi}$, where g is the gauge coupling of the dark group. The dark sector is decoupled from the standard model. We give the axion, which is displaced from its minimum, a simple UV-potential [1],

$$V(\phi) = \frac{1}{2}m^2\phi^2\,. \tag{3.2}$$

This potential intuitively illustrates the dynamics of our model, as the axion is essentially an overdamped harmonic oscillator. The interaction term $\mathcal{L}_{\rm int}$ adds an additional friction $\Upsilon(T_{\rm dr})$ to the equation of motion, dissipating energy through the production of dark radiation $\rho_{\rm dr}$ which is comprised of dark gauge bosons, where $T_{\rm dr}$ is the temperature of the dark radiation. In the small coupling limit ($\alpha \ll 1$), $m \ll \alpha^2 T_{\rm dr}$, and this friction can be inferred

[1] The IR potential from the confining group is rapidly suppressed at temperatures above the confining scale and we have checked that its contribution is sub-dominant for our parameters.

from the sphaleron rate for a pure non-Abelian gauge group [50, 73, 105] and scales as

$$\Upsilon(T_{\rm dr}) = \kappa\alpha^5 \frac{T_{\rm dr}^3}{f^2}\,, \tag{3.3}$$

where κ is an O(10) number[2] with weak dependence on α and $f > T_{\rm dr}$. The following equations of motion then describe the homogeneous evolution of the axion-radiation system:

$$\begin{aligned} \ddot{\phi} + (3H + \Upsilon\,(T_{\rm dr}))\,\dot{\phi} + m^2\phi &= 0 \\ \dot{\rho}_{\rm dr} + 4H\rho_{\rm dr} &= \Upsilon(T_{\rm dr})\dot{\phi}^2 \end{aligned} \tag{3.4}$$

where $\rho_{\rm dr} = \frac{\pi^2}{30} g_* T_{\rm dr}^4$ and $g_* = 7$ denotes the relativistic degrees of freedom in the new dark sector. ($g_* = 2(N^2-1)+1$ for a general SU(N), where the factor of 2 accounts for two gauge boson polarizations per gauge boson (N^2-1) and the axion contributes 1 additional degree of freedom.)

In the original EDE work, an oscillating scalar field subject only to Hubble friction had been proposed, whose energy must dilute like radiation or faster after the field becomes dynamical in order to diminish the Hubble tension. This requirement places rigid demands on the scalar-field potential $V \propto \left(1 - \cos\frac{\phi}{f}\right)^n$ considered by [26] (or $V \propto \phi^{2n}$ as in [98]) with $n \geq 2$. These potentials do not easily emerge from a UV-complete theory without extreme fine-tuning. Other proposed phenomenological EDE candidates [99] have similar fine-tuning issues.

In our DA model, the particle-production friction $\Upsilon \gg m, 3H$, overdamps the motion of the scalar field. Thus, because the field is not oscillating, its dynamics are not sensitive to the potential $V(\phi)$. Instead, the friction Υ extracts energy from the scalar field into the dark radiation, which automatically dilutes away as a^{-4}.

We approximate the solution to the equation of motion Eq. (3.4) as

$$\phi(z) \approx \phi_0 e^{-\frac{m^2}{H(z)\Upsilon(z)}}\,, \tag{3.5}$$

which is the solution to an overdamped oscillator where we approximated $t \simeq H(z)^{-1}$. Equation (3.5) illustrates that the DA begins to roll faster when $\frac{\Upsilon(z_d)}{m^2} \equiv H(z_d)$, where z_d

[2] For a general SU(N) κ increases with N. For details see [50].

denotes the redshift at which the axion field becomes dynamical. At high redshifts ($z \gg z_d$) the axion is slowly rolling, building up to a steady-state temperature on time scales of order Υ^{-1} in the dark sector,

$$T_{\rm dr}(z) \approx \left(\frac{m^4 f^2 \phi^2(z)}{2\frac{\pi^2}{30} g_* \kappa \alpha^5 H(z)} \right)^{\frac{1}{7}} , \tag{3.6}$$

by continuously extracting energy from the rolling field 2. As the field begins to roll faster, the temperature $T_{\rm dr}$ in the dark sector rises steadily and the field continuously dumps its energy into the dark radiation bath. However, due to the weak dependence of the temperature on the background quantities, this change is O(1). Therefore, approximating the friction $\Upsilon(z)$ as roughly constant does not change the qualitative behavior of our model at the background level, as we discuss in more detail in Sec. 3.2. Eventually, as the axion energy depletes, the source term $\Upsilon \dot{\phi}^2$ becomes smaller than $4H\rho_{\rm dr}$, leading to a decrease in temperature $T_{\rm dr}$ until $\Upsilon \dot{\phi}^2$ becomes negligible and the dark radiation dilutes away as a^{-4}.

The generation of a steady-state temperature is independent of the presence of an initial dark temperature, as even starting with temperature fluctuations of the order of Hubble is sufficient to rapidly build up to the temperature in Eq. (3.6) [19]. Indeed, the main features of the DA are universal in the presence of any large friction [$\Upsilon \gg H(z)$] for $\Upsilon \propto T^p$ with $p < 4$. The minimal model presented here has been explored in more detail [19] in the context of warm inflation [37, 38, 40, 46, 106, 107].

3.2 Background Dynamics

Having laid the groundwork for the background evolution of the DA , we turn to its ability to mimic EDE and draw comparisons with the best-fit parameters of Ref. [henceforth labeled P18]Poulin:2018cxd. The particle setup in Sec. 3.1 results in a rolling scalar field that behaves like a cosmological constant at early times plus a dark radiation component. The total contribution $\rho_{\rm DA}$ to an EDE-like component is then given by their sum

$$\rho_{\rm DA}(z) = \rho_\phi(z) + \rho_{\rm dr}(z), \tag{3.7}$$

where $\rho_\phi(z) \approx \frac{1}{2}m^2\phi^2(z)$[3]. At very early times, the radiation component is sub-dominant and ϕ is essentially frozen, acting like a cosmological constant giving

$$\rho_{\rm DA}(z \gg z_d) \approx \frac{1}{2}m^2\phi_0^2\,, \tag{3.8}$$

which is a function of only the axion potential and its initial conditions. Sometime after the axion thaws ($z < z_d$), the dark radiation becomes the dominant contributor to EDE as illustrated in Fig. 3.1. The DA constitutes a total fraction,

$$f_{\rm DA}(z) = \frac{\rho_{\rm DA}(z)}{\rho_m(z) + \rho_r(z) + \rho_{\rm DA}(z)} \tag{3.9}$$

of the energy density of the Universe, where ρ_m and ρ_r denote the matter and radiation densities. This fraction reaches a maximum at $z_{\rm peak}$. Relating this to the "critical redshift" z_c of the EDE as defined in P18, their best fit $z_c = 5345$[4] for the EDE that dilutes as radiation, which corresponds to $z_{\rm peak} = 3322$. Roughly at this time, the source term $\Upsilon\dot{\phi}^2$ in Eq. (3.4) becomes negligible, and the dark radiation dilutes away as a^{-4} as shown in Fig. 3.1.

By approximating the friction $\Upsilon(z_{\rm peak}) = \Upsilon_0$ as a constant, we illustrate how to estimate $z_{\rm peak}$ analytically. In this limit, the approximation for the temperature of the dark radiation simplifies to

$$T_{\rm dr}(z > z_{\rm peak}) \simeq \left(\frac{m^2\phi(z)}{2\sqrt{\frac{\pi^2}{30}g_* H(z)\Upsilon_0}}\right)^{\frac{1}{2}}, \tag{3.10}$$

which, using Eqs. (3.5) and (3.7), allows us to approximate $f_{\rm DA}$ as an analytical function in z,

$$f_{\rm DA}(z \geq z_{\rm peak}) \simeq \frac{e^{-\frac{2m^2}{H(z)\Upsilon_0}}\frac{1}{2}m^2\phi_0^2\left(1 + \frac{m^2}{2H(z)\Upsilon_0}\right)}{\rho_m(z) + \rho_r(z)}. \tag{3.11}$$

Solving $\frac{df_{\rm DA}}{dz}|_{z_{\rm peak}} = 0$, and assuming that the peak lies close to matter-radiation equality,

[3]The kinetic energy component of ϕ is negligible due to the large friction term.

[4]The posteriors for EDE parameters in P18 are non-Gaussian. The best-fit parameters quoted here therefore do not correspond to their mean values, and we hence do not include errors on these quotes.

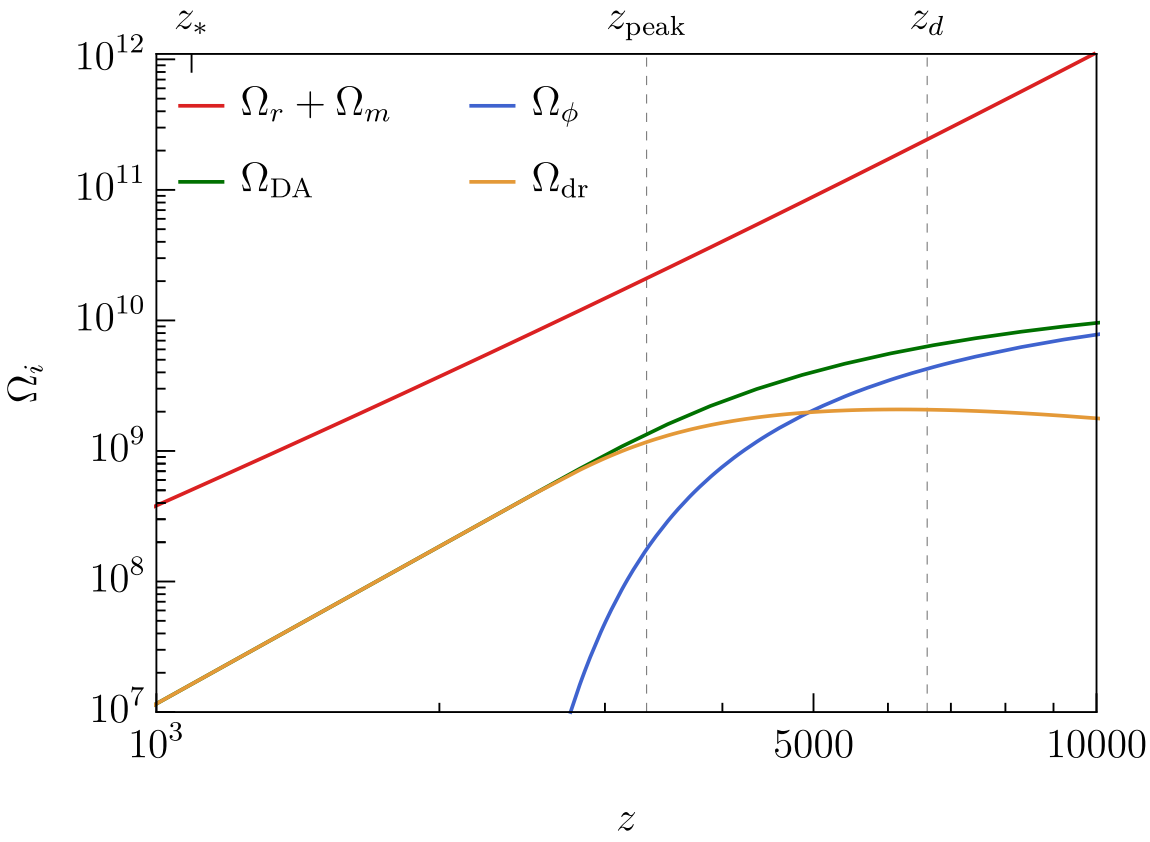

Figure 3.1: The fractional energy densities $\Omega_i = \rho_i/\rho_{\rm crit}$ of the different components in the DA and those in a ΛCDM universe, where $\rho_{\rm crit}$ is the critical density today. The total DA contribution (green) is a sum of its sub-components. At early times ($z \gg z_d$), the energy density Ω_ϕ in the scalar field (blue) is roughly constant and the dark radiation component $\Omega_{\rm dr}$ (yellow) is subdominant. At intermediate times ($z_{\rm peak} < z < z_d$), the dark radiation $\Omega_{\rm dr}$ transitions to become dominant as Ω_ϕ drops. Shortly after $T_{\rm dr}$ reaches a maximum, the total fractional DA energy density peaks at redshift $z_{\rm peak}$.

we can approximate $z_{\rm peak}$ as

$$z_{\rm peak} \simeq \left(\frac{1}{2\sqrt{\Omega_m}}\frac{m^2}{H_0\Upsilon_0}\right)^{\frac{2}{3}}, \tag{3.12}$$

where Ω_m is the fractional matter density today and $z_{\rm peak}$ is now dependent only on $\frac{\Upsilon_0}{m^2}$. Equations (3.10)−(3.12) demonstrate how the physical observables depend exclusively on $\frac{\Upsilon}{m^2}$, which sets the time scale at which the axion becomes dynamical, and $\frac{1}{2}m^2\phi_0^2$ which scales the total amount of early dark energy. Therefore, at the background level, we effectively introduce only two new parameters beyond ΛCDM, but expect the perturbations to depend on more than just these two parameters. Including the full temperature dependence of the friction at the background level requires solving the coupled differential Eq. (3.5) numerically by specifying an initial condition $\frac{\Upsilon(z_i)}{m^2}$ at some z_i, increasing the effective number of background parameters to three. While this does not have a significant impact on the qualitative behavior of the DA system, it does change $\frac{\Upsilon(z_i)}{m^2}$, and $\frac{1}{2}m^2\phi_0^2$ by O(1) when keeping $z_{\rm peak}$ and $f_{\rm DA}(z_{\rm peak})$ fixed.

For redshifts smaller than $z_{\rm peak}$, the early dark energy is dominated by the radiation component which dilutes as:

$$\rho_{\rm DA}(z < z_{\rm peak}) \simeq \rho_{\rm dr}(z_{\rm peak})\left(\frac{1+z}{1+z_{\rm peak}}\right)^4. \tag{3.13}$$

The fractional energy density $f_{\rm DA}$ is then peaked at $z_{\rm peak}$, as shown in Fig. 3.2. Our proposed model hence mimics the EDE proposed in P18 with $n = 2$, which resolves the Hubble tension.

The primary difference between the two models at the background level is a narrower peak for the DA (the effect being more pronounced for the constant friction approximation), as seen in Fig. 3.2. Based on this, we explore the expected differences between the background observables of the two models. In particular, we discuss the impact on CMB observables that capture the important features of the full CMB spectrum, but depend only on the background evolution of the Universe [24,96,108]. These are the size r_s of the sound horizon, the ratio $r_{\rm damp}/r_s$ of the damping scale to the sound horizon, the height of the first peak and the horizon size at matter-radiation equality.

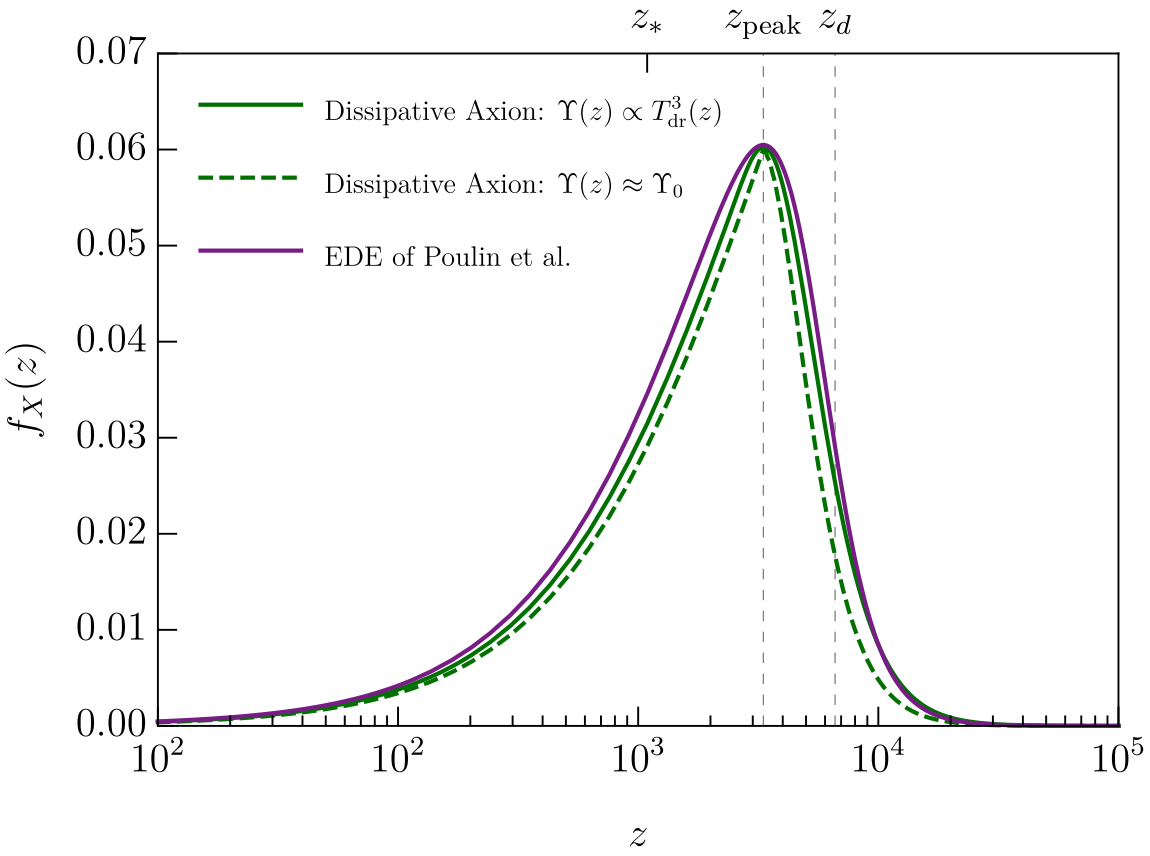

Figure 3.2: We compare the fractional extra energy density of the full temperature dependent DA model [$\Upsilon(z) \propto T_{\rm dr}^3$, solid green] with the semi-analytical approximations in equation (3.11) and (3.13), treating the friction as constant [$\Upsilon(z) \approx \Upsilon_0$ dashed green] and the EDE fluid approximation of an oscillating scalar field from Poulin et. al. [24] (purple). This plot uses the $n = 2$ EDE best-fit parameters [$z_{\rm c} = 5345, f_{\rm EDE}(z_{\rm c}) = 0.044$ which corresponds to $z_{\rm peak} = 3322$, $f_{\rm EDE}(z_{\rm peak}) = 0.060$] and dissipative axion parameters $\frac{\Upsilon(z_{\rm peak})}{m^2} = 1.3 * 10^{36}\,{\rm GeV}^{-1}$ $\left(\frac{\Upsilon_0}{m^2} = 5.7 * 10^{36}\ \ {\rm GeV}^{-1}\right)$, and $\frac{1}{2}m^2\phi_0^2 = 0.55\ \ {\rm eV}^4$ $\left(\frac{1}{2}m^2\phi_0^2 = 0.21\ \ {\rm eV}^4\right)$ for the temperature dependent (independent) DA model.

As our model adds more radiation to the Universe, we naively expect the redshift of matter-radiation equality to shift. Quantifying this shift correctly requires a full Markov chain Monte Carlo (MCMC) to allow other cosmological parameters, in particular the physical density $\omega_{\rm cdm}$ of cold dark matter to compensate for some or all of the shift. We expect that the results of the MCMC will pull our posteriors in a direction that minimizes change to $z_{\rm eq}$. We hence leave further discussion of changes to $z_{\rm eq}$ for future work. We expect an increase in $\omega_{\rm cdm}$ to similarly compensate for a change to the height of the first CMB peak. Such an increase was observed by P18 for EDE - the best-fit $\omega_{\rm cdm}$ increases by $\sim 9\%$ in the $n = 2$ EDE cosmology relative to ΛCDM. To compare, their maximum $f_{\rm EDE} \leq 7\%$. Moreover, the dark radiation peaks during matter-domination, further minimizing the effect of adding dark radiation to the Universe. Consequently, in this chapter, we limit our comparisons of the two models to investigating the effects of the sharper peak in $f_{\rm DA}$.

We first note that a slight narrowing of the peak of $f_{\rm DA}$ relative to $f_{\rm EDE}$ has minimal impact on the recombination redshift z_*. This was verified using a modified version of the equation of state parametrization of the EDE of P18, similar to Ref. [99], sharpening the peak in $f_{\rm EDE}$ and calculating z_* with the CLASS cosmology code [109, 110]. As z_* is a background quantity, and $f_{\rm DA}$ is nearly identical to a narrower $f_{\rm EDE}$, we expect z_* for the DA to be similar to the EDE scenario. Then, the main change to r_s comes not from the limits of its integral, but the integrand, specifically, the expansion rate. Knowing how the expansion rate for the DA differs from EDE, we can calculate r_s by fixing the background cosmology to the best fit of the $n = 2$ EDE of P18, and the DA parameters such that the temperature dependent (independent) $z_{\rm peak}$ and $f_{\rm DA}$ ($z_{\rm peak}$) match the best-fit EDE (values specified in the caption of Fig. 3.2), giving

$$r_s(z_*) = \int_{z_*}^{\infty} dz \frac{c_s(z)}{H(z)} = 140.0\,(140.1)\,\text{Mpc}\,, \tag{3.14}$$

compared to $r_s = 139.8\,\text{Mpc}$ in P18. Here, $c_s(z)$ is the speed of sound in plasma and the DA enters into the expansion rate $H(z)$. This is well within 1σ of the r_s in the best-fit EDE scenario of P18 for $n = 2$, for which the best-fit Hubble constant increases to $H_0 = 71.1$ km/s/Mpc. This along with a larger error on H_0 resolves the tension in the EDE case. As the CMB inferences of r_s and H_0 are degenerate, with a reduced r_s that matches P18 in the DA model, we similarly expect a high H_0 that will significantly ease the Hubble tension, if

not resolve it.

For $r_{\rm damp}$, we expect a smaller change still, as the integral for $r_{\rm damp}$ is sharply peaked close to recombination and less sensitive to the expansion rate $\sim z_{\rm eq}$. While the change in r_s is absorbed by H_0, thereby diminishing the Hubble tension, changes to $r_{\rm damp}/r_s$ can be absorbed by the tilt n_s of the primordial power spectrum as noted by Refs. [24, 96].

Another requirement of EDE models that succeed in resolving this discrepancy is an effective sound speed $c_s^2 < 1$ of perturbations in the new component [26, 98, 99]. This in part led to the success of Refs. [24, 26]. The DA model consists of a scalar field ($c_s^2 = 1$) and dark radiation ($c_s^2 = 1/3$) [111]. Although the coupling between the two components complicates matters, as $\rho_\phi < 20\%$ at $z_{\rm peak}$, the rest of the energy density being made up of dark radiation, naively, we expect c_s^2 for the DA to be between $1/3 < c_s^2 < 1$. Here, we simply seek to motivate the relevance of this model as a particle theory solution to the Hubble tension, and leave the exploration of perturbations to subsequent work. As the DA model produces a value for r_s extremely close to the EDE value, and little to no difference is expected in $r_{\rm damp}$ between the two models, these expectations coupled with the predicted increase in $\omega_{\rm cdm}$ make the DA a promising theoretical model to deliver the extra early dark energy component that can resolve the Hubble tension.

3.3 Discussion

In this chapter, we propose the DA as a particle-model solution to the Hubble tension. The axion couples to a dark non-Abelian gauge group[5], which adds an additional friction to the equation of motion of the axion and sources a dark radiation bath as the field rolls down its potential. This overdamped system has a well understood UV-completion and greatly alleviates the fine-tuning concerns present for the scalar-field EDE solutions. The injection time and total amount of added energy content is quantified fully by two linear combinations of parameters: $\frac{\Upsilon_0}{m^2}$ and $\frac{1}{2}m^2\phi_0^2$. The full theory has additional parameters, as the friction is determined by: $\Upsilon = \kappa\alpha^5\frac{T_{\rm dr}^3}{f^2}$. Here, κ is an O(10) number, $\alpha < 0.1$, $T_{\rm dr} < f$, and $m \ll \alpha^2 T_{\rm dr}$. For the sample values specified in the caption of Fig. 3.2, we find that these conditions are easily satisfied for many different combinations of viable parameters,

[5]We have focused on SU(2). A generalization to SU(N) only changes numerical factors for g_* and κ without qualitative impact.

for example: $m = 4 * 10^{-25}\,\mathrm{eV}$, $T_{\mathrm{dr}}(z_{\mathrm{peak}}) = 0.4\,\mathrm{eV}$, $f = 0.3\,\mathrm{GeV}$, $\alpha = 0.1$, $\phi_0 = 10^{-3} M_{\mathrm{Pl}}$, where M_{Pl} is the reduced Planck scale. We expect the full perturbative analysis to lift some of the degeneracy in these parameters and also in the choice of potential for the DA.

We have solely investigated the overdamped DA regime. Particle-sourcing friction could also play a role in an underdamped regime. Moreover, the DA can be theorized to have a UV-completion that ties its friction to the dark matter abundance. The symmetry breaking scale f can, for example, be linked to the presence of heavy quarks charged under the dark SU(N). Thus, the dark matter abundance could be determined by f, which also controls the friction Υ, potentially allowing a dynamical explanation for why the DA begins to roll close to matter-radiation equality. We leave a detailed exploration of this to future work.

We note that N_{eff} constraints will not restrict this model. While the CMB was emitted at the redshift of recombination, the peaks of the CMB spectra in fact encode information from redshifts $z \lesssim 10^6$ [101, 112]. The DA adds dark radiation to the Universe only after $\sim z_{\mathrm{eq}}$, unlike N_{eff} which adds radiation to the Universe at all times. Their imprints on the CMB peaks are hence different - the DA is expected to cause its largest change to the CMB close to the first peak in the TT spectrum based on Refs. [101, 112], while N_{eff} is not only constrained by matter-radiation equality, but also through its effect on the higher peaks in the CMB TT spectrum [113]. These distinct effects on the CMB imply that the DA model cannot be quantified by N_{eff}, nor be restricted by N_{eff} constraints.

Lastly, we have invoked the DA model here as an explanation of extra dark energy components that resolve the Hubble tension, but this model has applications far beyond this tension. It has already been shown to be a viable candidate for cosmic inflation 2, and could similarly drive the current cosmic acceleration (for example, [114]). A family of scalar fields have often been theorized to cause the two known eras of cosmic expansion [115, 116]. We add the DA to this list.

"I haven't failed. I've just found 10000 ways that won't work."

— Thomas A. Edison

Chapter 4

Decays of long-lived relics and their signatures at IceCube

The IceCube detector, located in the Antarctic ice layer, is sensitive to neutrino energies ranging from 10 - 10^{10} GeV [28]. Over its six year run, IceCube has detected several neutrinos in the energy range 30 TeV - 10 PeV [29–32, 117]. The measured neutrino flux in this range is significantly larger than that expected from the atmospheric neutrino background [29–32]. This suggests an alternative source with a significance of at least 7σ [33]. Previously, no statistically significant correlation between the direction of origin of the detected neutrinos and any known high energy γ-ray sources existed, suggesting an isotropic extra-galactic source [118]. Recently however, multi-messenger astrophysics linked one 290 TeV neutrino to a flaring blazar [119]. More data is necessary to determine whether blazars can explain the highest energy events. Other possible astrophysical sources such as Supernova remnants (SNRs), star forming regions, Fermi bubbles, and active galactic nuclei (AGNs), have also been considered in the past [120–128]. Beyond the standard model physics (BSM) explanations have been investigated with regard to heavy decaying dark matter (see, for example, [129–140]). However, many models of decaying dark matter as a source of the IceCube neutrinos are highly constrained because they are predicted to produce γ-rays in excess of current measurements [135,140,141]. In this chapter, we explore the

experimental signature of a heavy relic directly decaying to neutrinos, sourcing an isotropic extra-galactic high-energy neutrino flux. We focus on lifetimes that are shorter than the age of the universe. We examine whether this high-energy neutrino flux can fit the excess events seen between 250 TeV - 10 PeV. We show that many constraints imposed by γ-ray observations can be avoided under this set of assumptions.

Recently, electroweak corrections at energy scales well above the electroweak (EW) scale have drawn considerable attention [142–145]. For high-energy scattering and decays, the EW effects significantly impact phenomenology by producing higher multiplicity final states. Different implementation strategies have been explored with regards to heavy decaying DM [142, 146, 147]. In our analysis we implement a fixed order EW shower. We use the results of the shower to predict a neutrino spectrum and fit it to that detected at IceCube. We also explore how the decaying relic model is constrained by its impact on light element abundances, CMB anisotropies, and diffuse γ-ray spectra, after including the EW shower effects.

A long lived relic has been considered previously as a source for the IceCube neutrinos, and analyzed up to redshifts of $z = 1000$ [148, 149]. We extend this range by including neutrinos arising from re-scatterings off the relic neutrino background in our analysis. Our inclusion of EW corrections further changes the qualitative features of the neutrino flux today, leading us to conclude that EW corrections are a necessary part of an accurate forecast.

4.1 Models

In this chapter, we consider two models in which our relic, X, directly decays to neutrinos. In our analysis, the PeV-scale neutrinos observed at IceCube are assumed to come from these direct decays. Naively, one may wish to consider a toy-model decay: $X \to \overline{\nu}\nu$ [150]. However, implementing an EW shower highlights the inconsistency of this treatment. At ultra-high energies, the final state radiation includes many soft W's, which turn charged leptons into neutral ones and vice versa. This leads to the production of roughly the same amount of neutral and charged leptons for center-of-mass (COM) energies far beyond the EW scale. This is a side effect of unbroken isospin in the high-energy limit. Model-

independently, this implies that any high-energy neutrino spectrum sourced directly from a heavy relic decay will be accompanied by a spectrum of electromagnetically interacting particles, which will carry roughly the same amount of energy as the neutrino spectrum.

At energy scales much above the EW scale, Sudakov logarithms contribute to higher-multiplicity final states. These corrections grow logarithmically as the mass increases. Effectively this leads to the production of EW jets. To quantify the neutrino spectrum arising from these jets, we implement a fixed order EW shower. The qualitative features of the EW jets are model independent, as any heavy particle that decays to neutrinos will also radiate gauge bosons. To zeroth order, this effect takes a delta function centered around $\frac{M_X}{2}$, and smears it towards lower energies. The energy lost by the neutrinos is carried away by gauge bosons, which themselves can decay into neutrinos, and contribute to the neutrino spectrum at lower energies. We describe the implementation of the EW shower in detail in Appendix 4.6.

We consider two benchmark models that produce neutrinos through direct decays while remaining consistent with the isospin structure dictated by the Standard Model. We do not study a specific production mechanism for the heavy relic abundance, and assume it is cold. We note that inflationary dynamics can trivially produce such a particle during the reheating period [151]. Model-dependent constraints on these production mechanisms exist based on measurements such as isocurvature; however, these are not stringent enough to rule out the small abundance of decaying relics necessary to source the IceCube neutrinos [152, 153].

4.1.1 Model I: Heavy Scalar X_1

We consider a heavy scalar X_1, that couples to the standard model lepton doublets L^i. Here $i = 1, 2, 3$ indexes the generation. For simplicity, we assume flavor universality:

$$\mathcal{L}_1 = \frac{1}{2}\partial_\mu X_1 \partial^\mu X_1 - \frac{1}{2} M_X^2 X_1^2 + g_1 L^{i\dagger} \overline{\sigma}^\mu \partial_\mu L^i X_1 \tag{4.1}$$

The zeroth order decays are given by:

$$\begin{aligned} X_1 &\to \ell^+ \ell^- \\ X_1 &\to \overline{\nu_\ell} \nu_\ell \end{aligned} \tag{4.2}$$

The ratio of branching ratios is essentially 1 : 1 at tree level. We will refer to the above decay model I as $X \to \overline{\nu}\nu$.

4.1.2 Model II: Heavy Fermion X_2

In our second model we consider a heavy Dirac fermion, that couples to the standard model lepton doublets (L^i) and Higgs doublet (ϕ).

$$\mathcal{L}_2 = \frac{i}{2} X_2^\dagger \overline{\sigma}^\mu \partial_\mu X_2 - \frac{1}{2} M_X \left(X_2 X_2 + X_2^\dagger X_2^\dagger \right) + g_2 \phi^\dagger L^i X_2 + g_2^\dagger L^{i\dagger} \phi X_2^\dagger \tag{4.3}$$

We assume relic and its anti-particle have the same number density. The zeroth-order decays of X_2 are given by:

$$\begin{aligned} X_2 &\to \ell W, \\ X_2 &\to \nu_\ell Z/h, \end{aligned} \tag{4.4}$$

Again, the decays to $W^\pm, Z, h$ have equal branching ratios at tree-level in the high mass limit. We will refer to the above decay model II as $X \to V\ell$.

4.2 The Neutrino Spectrum

4.2.1 Derivation of the Present-Day Neutrino Flux

To derive the shape of the differential flux today we extend the analysis performed in [148]. We consider a number density of cold heavy relic Xs that decay with a given lifetime τ_X:

$$n_X(t) = n_{X,0}(t) \mathrm{e}^{-\frac{t}{\tau_X}}, \tag{4.5}$$

where $n_{X,0}(t)$ is the number density in the limit $\tau_X \to \infty$. For any given decay, high-energy neutrinos are injected into the thermal bath. The maximum possible energy is set by the mass of the heavy relic: $E_{\max} = \frac{M_X}{2}$. The fractional energy distribution $f_{E_{\max}}(x)$ of these neutrinos is determined by the EW shower, where $x = \frac{E}{E_{\max}}$ and E is the injection energy

of the neutrino. This decay gives rise to the following source term:

$$S_{\rm dec}(t,E) = n_X(t)\frac{1}{4\pi\tau_X}\frac{f_{E_{\rm max}}\left(\frac{E}{E_{\rm max}}\right)}{E_{\rm max}} \tag{4.6}$$

Depending on when they were produced, the neutrinos may free-stream or scatter off the relic neutrino background. The cross sections for all relevant (anti-)neutrino-(anti-)neutrino scattering processes are listed in [148]. The total scattering rate is determined by the thermally averaged cross section:

$$\Gamma_{\rm tot} = n_{\rm BG}\langle\sigma_{\rm tot}v_{\rm rel}\rangle \tag{4.7}$$

In the massless neutrino limit, the relative velocity simplifies to: $v_{\rm rel} = \frac{s}{2Ek}$, where s is the squared COM energy and k is the energy of the relic background neutrino. The scattering rate can then be written as [148]:

$$\begin{aligned}\Gamma_{\rm tot}(t,E) &= \frac{1}{16\pi^2E^2}\int dk\frac{1}{1+e^{\frac{k}{T_\nu(t)}}}\int_0^{4kE} dss\sigma_{\rm tot}(s) &(4.8)\\ &= \frac{T_\nu(t)}{\pi^2}\int dkk\ln\left(1+e^{-\frac{k}{T_\nu(t)}}\right)\sigma_{\rm tot}(s=4kE) &(4.9)\end{aligned}$$

where the second line is achieved via integration by parts. Neutrinos that scatter off the relic neutrino background, at the COM energies we consider, may produce two energetic neutrinos, two charged leptons, or two quarks. We define Γ_ν and σ_ν as the scattering rate and cross-section for $2\to 2$ neutrino scattering. We account for this re-injection of neutrinos by adding an additional source term. This is sometimes referred to as a tertiary source term [154].

$$S_{\rm ter}(t,E) = \int_E^\infty \frac{1}{\sigma_\nu(t,E')}\frac{d\sigma_\nu}{dE}\Gamma_\nu(t,E')\Phi(t,E')dE' \tag{4.10}$$

where $\Phi(t,E')$ is the differential neutrino flux defined in terms of the neutrino number density $n_\nu(t) = \int dE'\Phi(t,E')$, and E is the scattered neutrino energy.

We simplify equation (4.10) by rewriting the differential cross section in terms of the

injection energy, E', and the fractional scattered energy $y = E/E'$.

$$\frac{1}{\sigma_\nu}\frac{d\sigma_\nu}{dE} \approx \frac{1}{E'}\frac{1}{\sigma_\nu}\frac{d\sigma_\nu}{dy} \equiv \frac{1}{E'}g(y) \tag{4.11}$$

We can make the approximation in equation (4.11) because, for large boosts ($\gamma > 100$), $g(y)$ becomes independent of E'. We derive $g(y)$ by boosting the relevant differential cross sections from the COM-frame to the laboratory frame:

$$\frac{d\sigma_{\nu\nu}}{d\Omega_{\rm COM}} \propto 1 \tag{4.12}$$

$$\frac{d\sigma_{\bar{\nu}\nu}}{d\Omega_{\rm COM}} \propto (1+\cos\theta)^2 \tag{4.13}$$

Defining separate functions $g(y)$ for each scattering independently – for neutrino-neutrino scattering (and its conjugate scattering), $g_{\nu\nu}(y)$ and for the θ-dependent anti-neutrino-neutrino scattering (and its conjugate), $g_{\bar{\nu}\nu}(y)$ – we write:

$$g(y) = \frac{\Gamma_{\nu\nu}}{\Gamma_\nu}\left(g_{\nu\nu}(y) + g_{\nu\nu}(1-y)\right) + \frac{\Gamma_{\bar{\nu}\nu}}{\Gamma_\nu}\left(g_{\bar{\nu}\nu}(y) + g_{\bar{\nu}\nu}(1-y)\right) \tag{4.14}$$

where the ratios of scattering rates of $\nu\nu$ and $\bar{\nu}\nu$ are 0.6 and 0.4, respectively. We now can rewrite equation (4.10):

$$S_{\rm ter}(t,E) = \int_E^\infty g\left(\frac{E}{E'}\right)\frac{\Gamma_{\nu\nu}(t,E')\Phi(t,E')}{E'}dE' \tag{4.15}$$

We can now set up the Boltzman equation which describes the thermal evolution of the differential neutrino flux:

$$\frac{\partial\Phi}{\partial t} = -2H\Phi + HE\frac{\partial\Phi}{\partial E} + S_{\rm dec} + S_{\rm ter} - \Gamma_{\rm tot}\Phi \tag{4.16}$$

This partial differential equation can be solved numerically to obtain the present-day differential flux.

In our analysis, we implement a propagation code to track the cosmological evolution of individual neutrinos, which is equivalent to solving equation (4.16) in small time steps.

For a given lifetime τ_X we generate events over the appropriate distributions of redshifts, a decaying exponential. The energy spectrum of the injected neutrino is determined by the

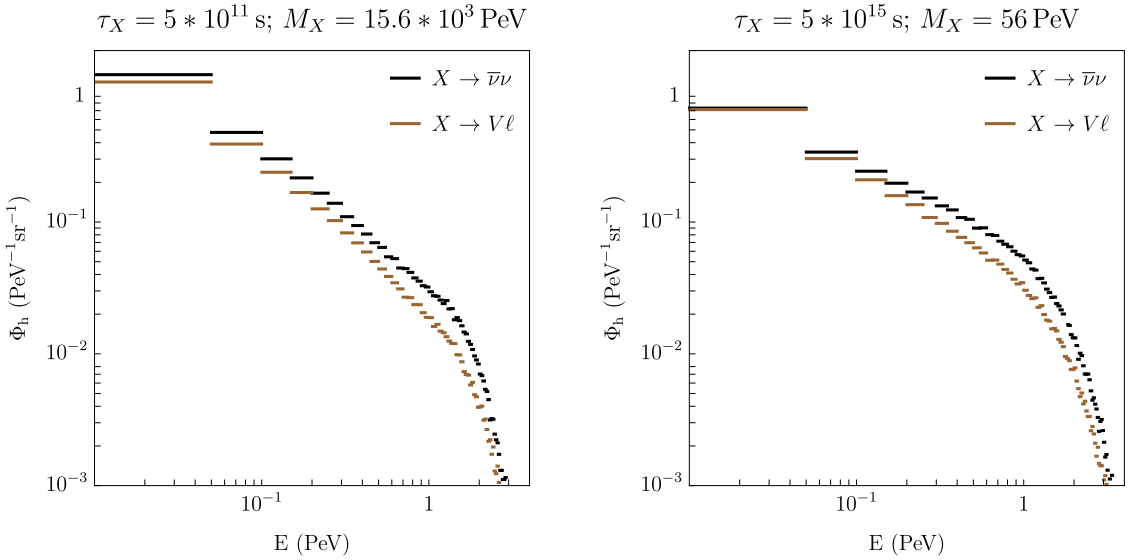

Figure 4.1: $\Phi_{\rm h}(t_0, E)$ for a heavy decaying relic X for two different lifetimes and two different decay models. The mass of X is set to $M_X = 2.4\,(1 + z_{\tau_X})$ PeV, the best fit mass of the neutrino spectrum measured at IceCube in the energy range $0.25 - 4$ PeV [31]. z_{τ_X} is the redshift z at the decay lifetime τ_X.

EW shower. Based on the decay redshift, z, we divide the total traveling time of the neutrino into intervals such that the average number of scatterings within the interval is much smaller than one. If a scattering event occurs within a time step, the probability of re-injecting two neutrinos with energy $g(y)$ and $g(1-y)$ is weighted by $\frac{\Gamma_\nu}{\Gamma_{\rm tot}}$. If two neutrinos are re-injected, they undergo the same treatment as the primary injection, starting at redshift z', where the scattering has occurred. This process iteratively continues until the neutrinos either arrive today or scatter into charged leptons or quarks.

The output of the simulation is a histogram $\Phi_{\rm h}(t_0, E)$, shown in Figure 4.1, which is related to the differential neutrino flux described in equation (4.16) by dividing by X's number density:

$$\Phi_{\rm h}(t_0, E) \equiv \Phi(t_0, E)/n_{X,0}(t_0) \tag{4.17}$$

where $\Phi(t_0, E)$ is the solution to (4.16) at $t = t_0$ and thus accounts for tertiary neutrinos and EW effects. For short lifetimes, including the tertiary neutrinos significantly enhances the flux of lower energy neutrinos, whereas for long lifetimes, these have negligible impact, since almost no scattering occurs. In the limit of negligible tertiary neutrinos, equation

(4.16) can be solved analytically [148].

In our analysis, we only account for neutrino fluxes emerging from extragalactic relic decays. Extragalactic decays are the only relevant neutrino source for relics with lifetimes $\tau_X \leq 8 * 10^{16}$s, while galactic decays become important when considering longer lived relics [135, 148, 155]. We leave a detailed investigation of that region of parameter space to future work.

4.2.2 Estimating X's Number Density

We use $\Phi_{\rm h}(t_0, E)$ to estimate the number density $n_{X,0}(t_0)$ needed to roughly produce the excess number of events seen in the high energy bins at IceCube [31]. The number of predicted events in this range at the IceCube detector is obtained by integrating over the differential flux times the effective area $A_{\rm eff}(E)$, which is provided by the IceCube collaboration [31], and multiplying by the detection time T (2078 days), and solid angle 4π, as well as the flux velocity $v = c$ to restore SI units.

$$N = \int_{E_{\rm min}}^{E_{\rm max}} \Phi(t_0, E) A_{\rm eff}(E) dE * 4\pi * v * T \tag{4.18}$$

Based of the total number of events ($N_t = 5$) in the range $0.25 - 4\,$PeV in [31] we estimate the number density $n_{X,0}(t_0)$ that is needed to produce the observed number of events:

$$n_{X,0}(t_0) = \frac{N_t}{\int_{E_{\rm min}}^{E_{\rm max}} \Phi_h(t_0, E) * A_{\rm eff}(E) dE * 4\pi * v * T} \tag{4.19}$$

4.3 Constraints

In the following sections we consider different observables that can be used to constrain heavy decaying relics, and how these constraints affect the relic models best suited to generate the PeV neutrinos observed at IceCube. The summary of our findings appear in Figure 4.2. The shortest lived relics, those with $\tau_X \leq 10^{12}\,$s, are most strongly constrained by their impact on the abundance of light elements generated during big bang nucleosynthesis (BBN). Relics with intermediate lifetimes, $10^{12}\,{\rm s} < \tau_X \leq 5 * 10^{15}\,$s, are most strongly constrained by their impact on the CMB anisotropy power spectrum. Relics with slightly

longer lifetimes, $5 * 10^{15}\,\mathrm{s} < \tau_X \leq 8 * 10^{16}\,\mathrm{s}$, are most strongly constrained by the γ-ray spectrum they generate. These constraints all depend on the amount of energy injected into the thermal bath in the form of electromagnetically interacting (EM) particles. In order to explore constraints on our relic models we define Ξ, the EM energy density produced by relic decays divided by the energy density of cold dark matter ρ_{CDM}:

$$\Xi \equiv f_{\mathrm{int}} \frac{n_{X,0} * M_X}{\rho_{\mathrm{CDM}}} \tag{4.20}$$

Here f_{int} is the fraction of the relic energy density that becomes EM energy and should in principle be redshift-dependent due to rescattering. However, for the parameter range we are considering, the dominant source of EM energy is from the decay shower where this fraction is largely M_X-independent. We take $M_X = 2.4\ (1 + z_{\tau_X})\,\mathrm{PeV}$, which gives the best fit mass for the two particular lifetimes shown in Figure 4.4, where z_{τ_X} is the redshift z at the decay lifetime τ_X. We use this mass as a benchmark for evaluating the constraints for all lifetimes shown in Figure 4.2.

Based on the results of the EW shower we estimate a conservative lower bound of $f_{\mathrm{int}} = 0.25$ for both decay models. This estimate assumes that about one third of all hadronic energy is electromagnetically interacting, as well as one third of the energy coming from muon and tau decays. This is the number we use for all constraints below.

4.3.1 Light Element Abundances

Helium-3 (He^3) and Deuterium (D) are produced during Big Bang Nucleosynthesis (BBN) and their measured abundances are in general agreement with the predictions of BBN (see review in [156]). Decays of heavy relics can initiate EM cascades that interact with the light elements and alter their abundances. Injected EM particles with energies above 27 MeV can participate in all of the photodisintegration processes pertinent to producing excess He^3 and D by destroying larger nuclei, primarily Helium-4 (He^4), as well as those that break He^3 and D down into protons [157–159]. Constraints arise from numerically following the evolution of the abundances of all light elements involved in the creation or destruction of He^3 and D, and comparing the end predicted abundances to the measured He^3 and D abundances [157, 158, 160–162]. This process, and the resultant constraints on a decaying particle injecting EM energy into the thermal bath, have already been worked out

in detail by [157, 158, 160–162]. We utilize those constraints on the allowed energy density and lifetime of a heavy decaying particle [162, 163].

4.3.2 CMB Anisotropies

EM energy injection by heavy decaying relics with lifetimes in the range $10^{12}\,\mathrm{s} \lesssim \tau_X \lesssim 5{*}10^{15}\,\mathrm{s}$ can increase the free electron fraction around recombination, thereby distorting the CMB anisotropy power spectrum. Detailed constraints have been worked out in [163, 164] and we rely heavily on their results, which utilize Monte Carlo Markov chains to calculate the effect of EM energy injection on the CMB anisotropy power spectrum. This study [163] rules out relics that inject enough EM energy at specific redshifts to produce power spectra inconsistent with current measurements.

The injection of EM energy increases the free electron fraction via ionization and collisional excitation. For relics with lifetimes of $10^{14}\,\mathrm{s} \lesssim \tau_X \lesssim 10^{18}\,\mathrm{s}$, the decays enhance the optical depth of the universe after recombination, leading to an additional suppression of the CMB temperature angular power spectra (TT) and polarization power spectra (EE) at small angular scales [163]. Additionally, the increase in the free electron fraction at times between recombination and reionization increases the probability that photons scatter before reionization. This leads to extra polarization, which creates a bump in the EE spectrum at smaller angular scales than the usual reionization bump [163].

Relics with lifetimes of $\sim 10^{13}\,\mathrm{s}$ are the most strongly constrained by the CMB anisotropy. The EM particles released by relics with lifetimes $\lesssim 10^{13}\,\mathrm{s}$ delay recombination. This widens the last scattering surface, damping the temperature power spectra at small angular scales. Like the longer lived particles mentioned above, particles with lifetimes $\tau_X \lesssim 10^{13}\,\mathrm{s}$ also generate a bump in the EE spectra to smaller angular scales than the usual reionization bump, though the effect is weaker than that generated by longer lived particles [163]. At times much earlier than $10^{13}\,\mathrm{s}$, the universe is fully ionized, and injection of electromagnetic particles, which increase the ionization fraction, have little impact. As a result, distortions to the CMB anisotropy spectum are exponentially suppressed for relics with τ_X much less than $10^{13}\,\mathrm{s}$. At lifetimes $\sim 10^{12}\,\mathrm{s}$, only a fraction of the relics decay late enough to alter the CMB and the constraints from CMB anisotropies become weaker than those that arising from BBN.

The analysis done by [163] only considers the effects of particles with kinetic energies in the range [10 keV, 1 TeV], well below the energies of EM particles relevant to our models. We argue that the bounds also apply to injected EM particles with $E \geq 1$ PeV because, around recombination, EM particles at these energies scatter off the CMB quickly enough to redistribute their energy to many particles with energies below 1 TeV, well within one Hubble time – energetic photons scatter off CMB photons via pair production extremely efficiently at these energies and redshifts. Electrons and positrons scatter off of the CMB through inverse Compton scattering, which while less efficient than pair production at these energies, is still much faster than the Hubble expansion rate for electrons of all energies considered in this chapter, as can be verified.

Different injection energies in the range between [10 keV, 1 TeV] have different efficiency factors determined by their interactions with the thermal bath, which sets the width of the constraints in [163]. To know exactly where within this band our injection energies lie one would have to do a dedicated study. Here, we conservatively apply the least stringent bounds, which correspond to the lowest efficiency of dumping the electromagnetic energy into the thermal bath, noting that a dedicated study for our particular injection energies may improve these bounds by up to a factor of five.

4.3.3 γ-Ray Constraints

When the heavy relic decays, the EW shower and decays of the showering products produce energetic photons, electrons, and positrons. These are reprocessed, producing a lower energy γ-ray distribution, primarily by inverse Compton scattering and pair production [166]. The γ-rays in this reprocessed spectrum lie in the energy range visible to the Fermi telescope, between 0.1 GeV and 820 GeV [167]. We derive constraints by requiring that the reprocessed spectra of heavy relic decays produce a γ-ray flux that is, in any bin, no more than 2σ above the flux presented in the Fermi Pass 7 Isotropic Extragalactic Gamma Ray (IGRB) spectrum [167].

In order to derive the reprocessed γ-ray spectrum resulting from a heavy relic decay, we follow [166,168]. Processes by which γ-rays can lose energy include photoioization, Compton scattering, photon matter pair production, and scattering off of the CMB. In this analysis, we approximate the γ-ray spectra as if EM particles are only reprocessed by the dominant

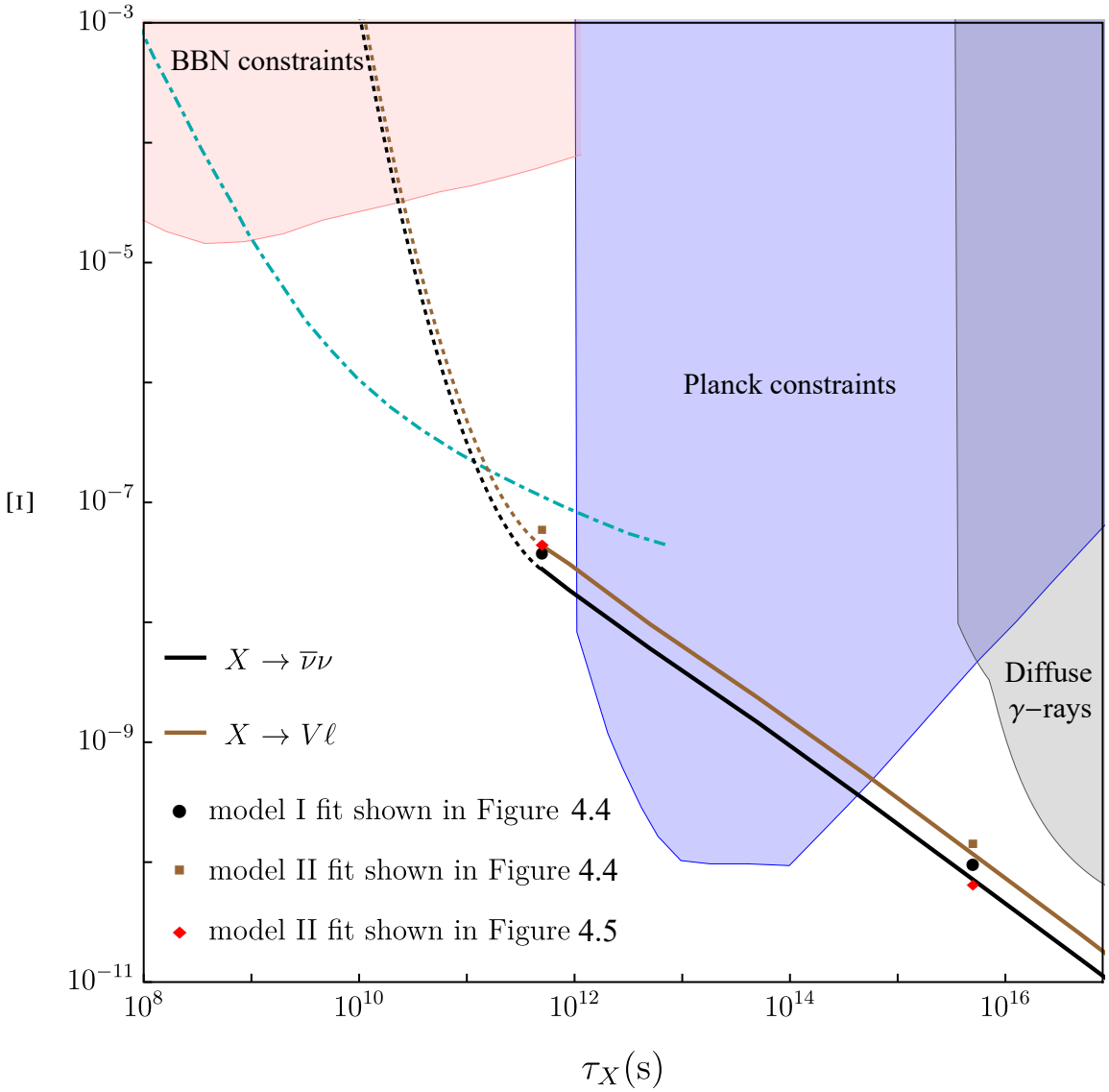

Figure 4.2: Constraints on a wide array of different lifetimes for a heavy decaying relic X, releasing EM energy into the thermal bath. All constraints are at 95% confidence level. The light red shaded area is excluded by measurements of light element abundances and their agreement with BBN predictions. The blue shaded area is excluded by bounds from CMB anisotropies. The gray shaded region is excluded by diffuse γ-ray observations. All of these constraints are for injections of EM energy above some threshold value unique to the constraint and described in their respective sections of this chapter. The cyan line is the forecast from the proposed PIXIE experiment, which could place more stringent bounds from y-distortion [165]. The black and brown lines indicate the abundance necessary to produce the excess IceCube neutrinos for models I and II, based off equation (4.19) and (4.20), assuming $M_X = 2.4\,(1+z_{\tau_X})\,\mathrm{PeV}$. The black and brown (red) markers indicate the data points corresponding to the IceCube spectrum shown in Figure 4.4 (Figure 4.6). The dotted lines indicate $M_X = 2.4\,(1+z_{\tau_X})\,\mathrm{PeV}$ transitioning to an approximation rather than a best fit, as rescattering effects can change the electromagnetic fraction by $\mathcal{O}(1)$.

scattering mechanisms for a particular redshift and energy. We also assume that a photon does not scatter if it has an optical depth $d_\tau < 1$. In this context, the optical depth can roughly be thought of the average number of times a photon scatters as it travels toward the Earth.

For redshifts $0 < z \leq 700$, EM particles are reprocessed by initiating cascades with CMB photons through pair production and photon-photon scattering [166]. Pair production is generally more efficient at reprocessing EM particles, except in a small range of energies for $300 \leq z \leq 700$, in which photon-photon scattering is more efficient. Photon-photon scattering has a negligible effect on the constraints of relics with $\tau_X \geq 5 * 10^{15}$ s, so we only consider the effect of pair production cascades in this analysis. In pair production cascades, photons pair produce electrons and positrons with CMB photons. The resulting electrons and positrons then upscatter CMB photons by inverse Compton scattering. These two processes continue until the COM energy falls below the pair production threshold. EM particles with energies above the threshold [166, 168]:

$$E_{\rm th}(z) = \frac{m_e^2}{30\ {\rm T}(z)} \approx \frac{36\ {\rm TeV}}{1+z} \tag{4.21}$$

have an optical depth $d_\tau > 1$. Particles with energies below $E_{\rm th}$ have optical depths $d_\tau < 1$, in which case we assume they free-stream toward the earth. At $z > 700$, additional scattering processes become important and all EM particles relevant to this analysis thermalize and do not produce any γ-rays observable today [166].

Since the particle cascades occur quickly compared to the expansion rate of the universe [168], we define a universal 'instantaneously' generated differential γ-ray cascade spectrum per unit injection energy[1] $\mathcal{L}(E, z)$, such that $N_\gamma = E_{\rm inj} \int \mathcal{L}(E, z) dE$, where N_γ is the number of γ-rays produced when $E_{\rm inj}$ of energy is injected into the thermal bath at redshift z. $\mathcal{L}(E, z)$ is built into the source term in the Boltzmann equation describing the evolution of the differential γ-ray flux:

$$\frac{\partial \Phi_\gamma}{\partial t} = -2H\Phi_\gamma + HE\frac{\partial \Phi_\gamma}{\partial E} + S_\gamma \tag{4.22}$$

where S_γ is the source term and H is the Hubble parameter. For a heavy relic, whose

[1] Note that our definition differs from the one given in [166].

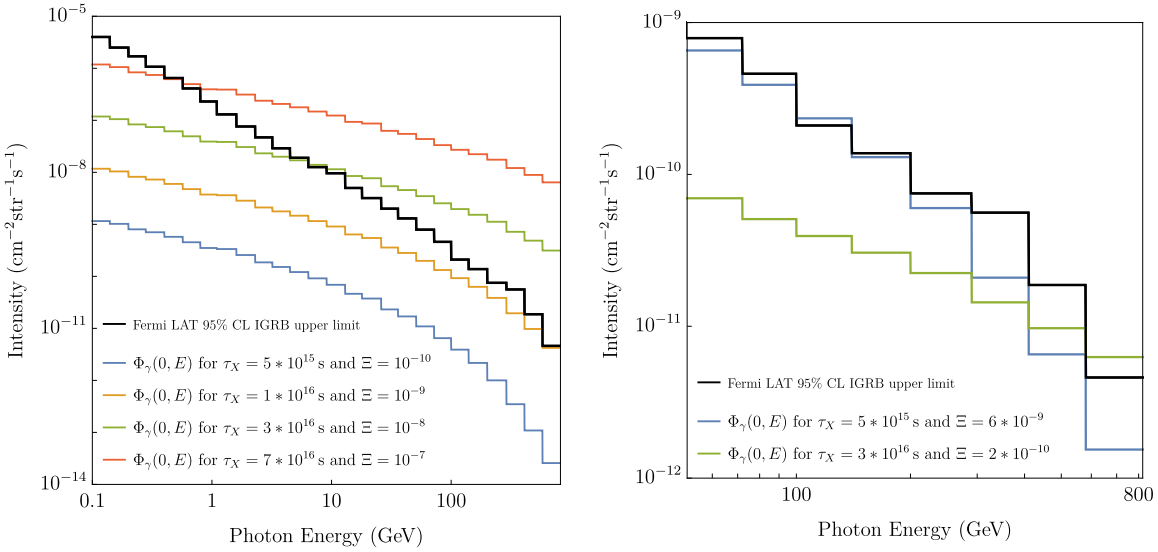

Figure 4.3: Comparison of the Fermi LAT 95% CL IGRB upper limit with the derived diffuse isotropic γ-ray flux $\Phi_\gamma(0, E)$ produced by a decaying heavy relic X for different lifetimes and abundances. The blue line in the left plot corresponds to the black dot in Figure 4.2, which is the abundance necessary to obtain the model I fit shown in Figure 4.4. Since $\Phi_\gamma(0, E)$ scales linearly in intensity with Ξ the spectra for the brown dot (model II fit shown in Figure 4.4) and red dot (model II fit shown in Figure 4.6) can be obtained by multiplying the blue line by a factor of $\frac{7}{5}$ and $\frac{2}{3}$, respectively. Shorter lifetimes ($\lessapprox 8 * 10^{15}$ s) are most stringently constraint by the energy range between 100-140 GeV. For longer lifetimes the highest energy range from 580-820 GeV has the highest constraining power.

decays initiate EM cascades, the source term is:

$$S_\gamma(t,E) = \frac{1}{4\pi}\frac{M_X f_{\rm int}}{\tau_X} n_{X,0}(t_0) e^{-\frac{t}{\tau_X}} \left(1+z(t)\right)^3 \mathcal{L}(E,z(t)) \tag{4.23}$$

Here we use $M_X f_{\rm int}$ to denote the total EM energy injected per relic decay[2]. Solving the above Boltzmann equation (4.22), gives the diffuse γ-ray flux for any given z.

$$\Phi_\gamma(z,E) = \frac{M_X n_{X,0} f_{\rm int}(1+z)^2}{4\pi\tau_X}\int_z^{700}\frac{dz'}{H(z')}\mathcal{L}\left(E\frac{1+z'}{1+z},z'\right)e^{-\frac{t(z')}{\tau_X}} \tag{4.24}$$

For observational purposes, we are interested in the flux at $z=0$. We compare the derived diffuse γ-ray flux today, $\Phi_\gamma(0,E)$, for different lifetimes and abundances in Figure 4.3.

$$\Phi_\gamma(0,E) = \Xi * \frac{\rho_{CDM}}{4\pi\tau_X}\int_0^{700}\frac{dz'}{H(z')}\mathcal{L}\left(E(1+z'),z'\right)e^{-\frac{t(z')}{\tau_X}} \tag{4.25}$$

$\mathcal{L}(E,z)$ depends on the dominant scattering process for a given redshift. The cascade spectrum for pair production was numerically calculated by [169]. Here, we use an approximate result only taking into account pair production (as the effects where photon-photon scattering is dominant are negligible):

$$\mathcal{L}(E_\gamma,z) = \begin{cases} 0.767 E_{\rm th}(z)^{-0.5} E_\gamma^{-1.5}, & 0 \le E_\gamma < 0.04 E_{\rm th}(z) \text{ and } z < 700 \\ 0.292 E_{\rm th}(z)^{-0.2} E_\gamma^{-1.8}, & 0.04 E_{\rm th}(z) \le E_\gamma < E_{\rm th}(z) \text{ and } z < 700 \\ 0, & E_{\rm th}(z) \le E_\gamma \text{ or } z \ge 700 \end{cases} \tag{4.26}$$

We derive constraints by comparing γ-ray spectrum that results from relic decay to the Fermi IGRB spectrum [167], requiring the predicted relic contribution produces less than a 2σ contribution in any one bin as illustrated in Figure 4.3. Our results are shown in Figure 4.2.

[2]In defining this source term we assume that all EM particles that result from relic decay are energetic enough to initiate a particle cascade. In general, one would need to consider a source term where the fraction of the relic mass energy that becomes EM particles capable of initiating a cascade depends on z.

4.3.4 Other Constraints

Spectral distortions to the CMB are often used to constrain the release of EM energy in the early universe [170,171]. These constraints can be derived by requiring that the decaying relic not produce μ- and y- distortions larger than the detection limit of COBE-FIRAS [172]. These are weaker than the constraints that arise from the light element abundances for the same redshifts, and thus not relevant for this analysis. However, as shown in figure 4.2, the proposed Primordial Inflation Explorer (PIXIE) [165], with projected sensitivities to μ- and y-distortions $\sim$ 1000x better than those of COBE-FIRAS, could detect y-distortions generated by almost all of the heavy relic models considered in the shorter lifetime parameter space window.

Other works consider constraints on BSM physics from the 21 cm spin temperature signal [163,173,174]. A heavy decaying relic would heat the intergalactic medium, resulting in a positive change to the differential brightness temperature. We do not consider these constraints in detail in this chapter because rough estimates in [163] indicate that they are not currently powerful enough to be relevant. However, more data and improvements in the uncertainty of the differential brightness temperature measurement could eventually provide stronger constraints [173, 175].

4.4 Comparison to IceCube Data

Figure 4.2 shows that there are two windows in which a heavy decaying relic could be the source of the PeV neutrinos observed at IceCube, one with longer lifetimes from $5*10^{14}$ s to $8*10^{16}$ s, and one with shorter lifetimes between $7*10^{10}$ s and 10^{12} s . Here, we show the full neutrino spectrum predicted by the decay of a heavy relic, including neutrinos that result from EW-showering and re-scattering off of the relic neutrino background, for two sample lifetimes within these two allowed ranges. We compare these spectra to six years of IceCube data and we consider data from two different datasets. The first dataset (DS1) includes neutrinos of all flavors that deposited their energy within the detector [31]. The second dataset (DS2) considers six years of IceCube data on upward going muon neutrinos, where the interaction vertex was also allowed to be outside of the detector, significantly enhancing the effective area [32]. Both datasets are complementary, and predict roughly

the same neutrino fluxes for energies above $3 * 10^5$ GeV [32]. The main focus on our analysis has been on DS1. We still include DS2 in our analysis because it contains the highest energy neutrino event measured to date. The event, which deposited 4.5 PeV in the detector, has a 88% probability of being caused by a muon-neutrino, in which case IceCube predicts a reconstructed energy of 7.5 PeV [32]. All other anomalous high-energy neutrino events in both data sets have energies below 2.5 PeV. We show the best fit for two allowed sample lifetimes for DS1 [31]. We also show the best fit to all of the data by combining both datasets. We want to stress that the IceCube collaboration has not published a combined measurement, and thus our second set of fits should be taken as purely illustrative.

For the following comparison, we choose to fit only to the highest energy events even though there also exists an excess in the lower energy range. We make that choice because a decaying relic cannot comfortably explain both of these excesses at the same time. Other works have considered astrophysical explanations, such as pulsar wind nebulae, Fermi bubbles, and unidentified galactic TeV sources, for this lower energy excess [125, 127, 176]. One should note that systematic uncertainties and atmospheric backgrounds are much higher in the lower energy range than the higher energy range. Additionally, DS1 and DS2 are in tension for bins below $3 * 10^5$ GeV [32]. The excess of events in the lower energy range is larger in DS1 than in DS2. A better understanding of the tension between the two datasets in this range may be able to give additional insight into the source of the lower energy excess.

4.4.1 Dataset 1

Here, we compare our forecast to DS1 [31]. Figure 4.4 shows the neutrino spectrum forecast with the best fit mass to DS1 for two different allowed lifetimes $\tau_{X_s} = 5 * 10^{11}$ s and $\tau_{X_l} = 5 * 10^{15}$ s. We choose the mass such that the chi-squared is minimized within the range $2.5 * 10^5$ GeV - $4 * 10^6$ GeV [31]. We can see that for both allowed lifetimes, the spectrum resulting from a heavy decaying relic can reproduce the four highest energy non-zero bins reasonably well. Qualitatively, the spectra do not differ much between the different lifetimes. The shorter lifetime τ_{X_s} predicts slightly more events between $2.5 * 10^5$ GeV - $4 * 10^5$ GeV, which is an indicator of tertiary neutrinos contributing to the lower tail of the spectrum. While overall there is some contribution to the lower energy bins between $6 * 10^4$ GeV -

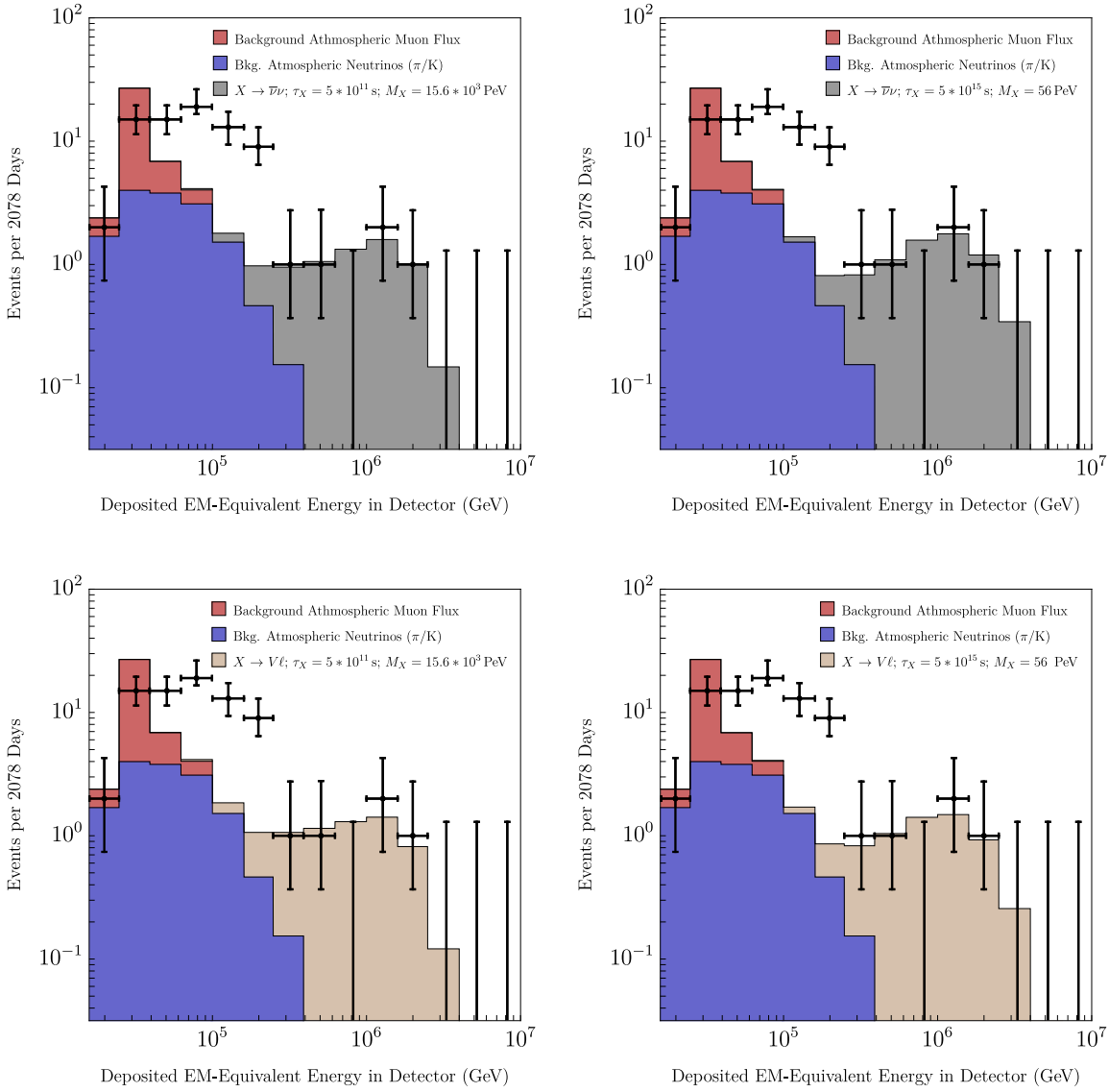

Figure 4.4: Neutrino spectrum forecast for decay model I and II for two different allowed lifetimes. The displayed spectrum shows the best mass fit for the $0.250 - 4\,\mathrm{PeV}$ neutrinos to DS1 for a short sample lifetime $\tau_{X_s} = 5 * 10^{11}\,\mathrm{s}$ on the left, and a long sample lifetime $\tau_{X_l} = 5 * 10^{15}\,\mathrm{s}$ on the right.

$2.5 * 10^5$ GeV, which relieves some of the tension between the expected background and the measurement, it is still an order of magnitude too small to be in agreement with the data. This suggests that different sources or systematic backgrounds would be needed to explain the excess seen between $5 * 10^4$ GeV - $2.5 * 10^5$ GeV.

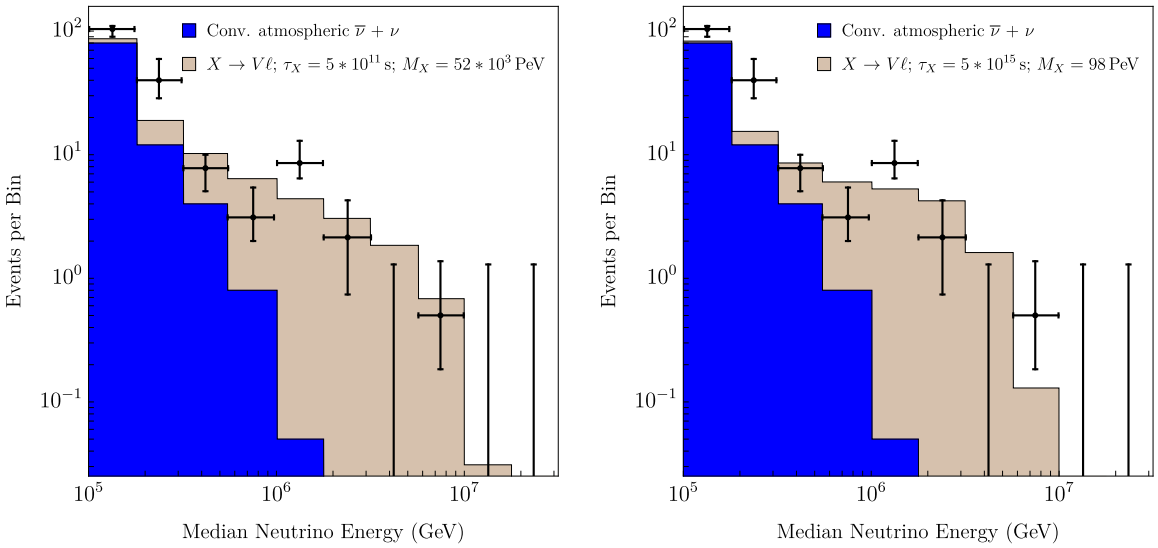

Figure 4.5: Neutrino spectrum forecast from decay model II ($V \to V\ell$) for two different allowed lifetimes. The displayed spectrum shows the best mass fit in the range 0.3 PeV - 10 PeV to the combined dataset for a short sample lifetime $\tau_{X_s} = 5 * 10^{11}$ s on the left, and a long sample lifetime $\tau_{X_l} = 5 * 10^{15}$ s on the right.

4.4.2 Combined Datasets 1 and 2

To combine both datasets, we rearrange equation (4.18) to find the average flux per bin Φ_a as predicted by the number of events per bin, N_b, in DS1:

$$\Phi_a = \frac{N_b}{\int_{E_{\min}}^{E_{\max}} dE\, A_{eff}(E) * 4\pi * v * T} \tag{4.27}$$

$E_{\min}$ and $E_{\min}$ correspond to the lower and upper limit in each bin in DS1. We consider all bins between $2.5 * 10^5$ GeV - 10^7 GeV. We then calculate how many events per bin, N_p,

the average flux Φ_a predicts in DS2:

$$N_p = \int_{E'_{\min}}^{E'_{\max}} dE\, \Phi_a A'_{eff}(E) * 2\pi * v * T * \eta_f \tag{4.28}$$

$E'_{\min}$ and $E'_{\max}$ correspond to the lower and upper limit in each bin in DS2. $A'_{eff}(E)$ is the effective detection area for DS2 provided in [32]. $\eta_f = \frac{1}{3}$ is the flavor efficiency factor, accounting for DS2 only being sensitive to muon-neutrinos.

Combining both datasets shifts the best mass fit from $M_X = 2.4\,(1 + z_{\tau_X})$ PeV to $M_X = 8.\,\left(1 + z_{\tau_{X_s}}\right)$ PeV and $M_X = 4.4\,\left(1 + z_{\tau_{X_l}}\right)$ PeV for the short ($\tau_{X_s} = 5 * 10^{11}\,\mathrm{s}$) and long ($\tau_{X_l} = 5 * 10^{15}\,\mathrm{s}$) lifetimes, respectively. Non-surprisingly, including the higher energy event shifts the mass fits towards higher masses. While for the longer lifetime the spectrum shape still shows the remains of a peak centered around $E_{\max}$, the spectrum for the shorter lifetime does not show this feature. This is due to the spectrum being dominated by tertiary neutrinos, which leads to a power-law shape with a hard cut-off. This effect is more pronounced in the combined dataset fit for τ_{X_s}, because higher M_X enhances the scattering rate off of relic neutrinos.

4.5 Conclusion

We utilize EW corrections to constrain heavy decaying relic abundances, using measurements impacted by EM energy injection, such as light element abundances during BBN, CMB anisotropies, and diffuse γ-ray spectra. Beyond the scope of our application, in the future EW corrections may be a useful tool to better constrain BSM physics beyond collider reach, using cosmological and astrophysical data.

We derive a precise forecast of neutrino spectra produced by direct decays from heavy relic particles with lifetimes smaller than $\tau_X < 8 * 10^{16}\,\mathrm{s}$. Due to our analysis including EW showers and tertiary neutrinos, our forecast accurately captures the shape of the possible spectra, and thus can be used as a powerful discriminant against other astrophysical explanations. This will prove useful as IceCube collects more data. IceCube has plans for a large expansion of its detecting abilities referred to as IceCube Gen 2 [177]. These include plans to increase IceCube's detection area by a factor of 10, which is expected to improve

IceCube's detection sensitivity for neutrinos with energies in the range 10 TeV -1 EeV by a factor of 10 [177].

Further, we can expect future experiments to shed more insight into the decaying relics proposed here. PIXIE should be able to detect y-distortions from relics with $\tau_X \lesssim 5 * 10^{11}$ s.

Any isotropic, long lived decaying relic heavy enough to generate 1 PeV neutrinos will also produce a unique γ-ray spectrum. While Figure 4.2 reveals that none of the decaying relics considered in this chapter are ruled out by their γ-ray spectra, this may change as Fermi's detection resolution improves, and as more sensitive γ-ray telescopes come online. The latest Fermi data analysis, Pass 8, is far more sensitive to point sources than Pass 7, and additional analysis seem to indicate that much of the IGRB flux derived from Pass 7 may actually be unresolved point sources [178]. Considering the analysis done by [178], we conservatively estimate that at least half of the IGRB flux measured in Pass 7 is actually unresolved point sources. This would tighten the γ-ray constraints by at least a factor of 2. However, [178] contends that the entire IGRB measured in Pass 7 could in principle be explained by unresolved point sources, suggesting that the γ-ray constraints could become significantly tighter, depending on what fraction of the IGRB is eventually found to be unresolved point sources. These constraints will also improve as γ-ray telescopes with better point source resolution, such as the High Energy Cosmic Radiation Detection facility (HERD) and the Chernekov Telescope Array (CTA), come online in 2020 with expected 10x more sensitivity than current γ-ray detectors [179].

If most point-source contributions to the IGRB are identified, what remains might be a truly isotropic spectrum from a model such as those described here. Thus, more IceCube data, paired with improved γ-ray detection sensitivity, may provide a smoking gun for confirming a heavy decaying relic as source of the IceCube neutrinos and thus physics beyond the standard model.

4.6 Electroweak Showering

At energies much larger than the electroweak scale, electroweak radiative corrections have a large impact on decay and scattering processes. This has been explored in the liter-

ature with regards to a 100 TeV particle collider [143], and indirect dark matter detection spectra [142]. These radiative corrections can be approximated by factorizing the differential cross section (or decay width) into the original $2 \to 2$ ($1 \to 2$) process, times the differential probability that one of the final states will emit an additional gauge boson (or split into two different particles altogether).

At very high energies there will be more splittings, which requires a summation for a full treatment. However, the majority of the higher order splittings are soft, which means they only carry a small fraction of the total energy. To compare our prediction to the spectrum at IceCube we are only interested in neutrinos within two orders of magnitude of the highest energy neutrinos. This allows us to use a cutoff above which the splitting probability does not exceed 1. In our EW shower we only consider 'hard' first order splittings, in which the gauge boson carries more than 10^{-2} of the maximum possible energy. This treatment captures how the resulting spectrum today is affected by the additional particles produced by a decay. However, at these high COM energies, many soft W's can populate the final state, which can turn a charged particle into a neutral one and vice versa. Therefore at high energies we keep track of all leptons and scalars (for the Higgs and the longitudinal components of the gauge bosons), and do an isospin average in the end.

We use the following splitting functions in the implementation of the EW shower. Here we follow the notation in [142]. $D_{A\to B}(x)$ gives the differential probability that a particle A turns into another particle B, with fraction x of the initial energy. Equations (4.31)-(4.37) show the splitting functions for scalars such as the Higgs h, and the longitudinal components of the gauge bosons, W_L and Z_L. Equations (4.38)-(4.42) show the splitting functions for fermions. All couplings are renormalized. $L(x)$ and l below are the universal kinematical functions [142]:

$$L(x) = \ln \frac{sx^2}{4M_V^2} + 2\ln\left(1 + \sqrt{1 - \frac{4m_V^2}{sx^2}}\right) \tag{4.29}$$

$$l = \ln \frac{s}{M_V^2} \tag{4.30}$$

Splitting Functions for h/Z_L

In the following equations h may be replaced with Z_L. In the high-energy limit h and Z_L are not distinguishable, which is why they have the same splitting functions.

$$D_{h\to W_T}(x) = \frac{\alpha_2}{2\pi}\frac{1-x}{x}L(x) \tag{4.31}$$

$$D_{h\to Z_T}(x) = \frac{\alpha_2 c_w^2}{\pi}\frac{1-x}{x}L(x) \tag{4.32}$$

$$D_{h\to t}(x) = \frac{3\alpha_t}{2\pi}l \tag{4.33}$$

Notice that the initial particle spin stays the same when emitting a gauge boson. Here for example we start out with a Higgs H, which can emit a W_T, which turns the Higgs into a W_L, or it can emit a Z_L, in which case it remains a Higgs. In either case the mother-particle, which carries the majority of the energy after the splitting, remains a scalar. The Higgs can also split into two top quarks, in which case neither of them have a higher probability of carrying the majority of the energy. This can be seen by 4.33 being independent of x. (Splittings into other quarks and leptons are negligible because their yukawa couplings are small.)

Splitting functions for W_L

$$D_{W_L\to W_T}(x) = \frac{\alpha_2}{2\pi}\frac{1-x}{x}L(x) \tag{4.34}$$

$$D_{W_L\to Z_T}(x) = \frac{\alpha_2}{\pi}\frac{(s_w^2-\frac{1}{2})^2}{c_w^2}\frac{1-x}{x}L(x) \tag{4.35}$$

$$D_{W_L\to\gamma}(x) = \frac{\alpha_{EM}}{\pi}\frac{1-x}{x}L(x) \tag{4.36}$$

$$D_{W_L\to t}(x) = \frac{3\alpha_t}{4\pi}l \tag{4.37}$$

Splitting functions for fermions

Here are the splitting functions for a charged fermion:

$$D_{f\to W_T}(x) = \frac{\alpha_2}{2\pi}\frac{1}{2}\frac{1+(1-x)^2}{x}L(x) \tag{4.38}$$

$$D_{f\to Z_T}(x) = \frac{\alpha_2}{2\pi}\frac{1}{4c_w^2}\frac{1+(1-x)^2}{x}L(x) \tag{4.39}$$

$$D_{f\to \gamma}(x) = \frac{\alpha_{EM}}{2\pi}\frac{1}{4c_w^2}\frac{1+(1-x)^2}{x}L(x) \tag{4.40}$$

Here are the splitting functions for a neutral fermion:

$$D_{f\to W_T}(x) = \frac{\alpha_2}{2\pi}\frac{1}{2}\frac{1+(1-x)^2}{x}L(x) \tag{4.41}$$

$$D_{f\to Z_T}(x) = \frac{\alpha_2}{2\pi}\frac{(s_w^2-\frac{1}{2})^2}{c_w^2}L(x) \tag{4.42}$$

Description of Included Processes

In model I, each decay produces two leptons. In model II, each decay of a heavy X-particle produces one scalar and one lepton. We consider one hard splitting off of both daughter particles. We decay all top quarks, keeping track of all gauge bosons. We combine the energy spectrum of the primary lepton with subsequent decays from any gauge bosons (V_L and V_T) to secondary leptons. We consider only direct leptonic decays, as neutrinos resulting from hadronic decays are much less likely to be energetic enough to be above our set threshold of $x > 0.01$. Included gauge bosons come from the primary scalar, radiation off of either leptons or scalars, and subsequent decays from top quarks to W's.

The total lepton spectrum $f_{\text{tot}}(x)$ is the combination of the primary and secondary lepton spectrum. $f_{\text{tot}}(x)$ is the probability distribution of producing a lepton with fraction x of $\frac{M_X}{2}$. Since we have to average over charged and neutral leptons due to the possibility of soft W-emission, the probability distribution of a neutrino with energy fraction x of $\frac{M_X}{2}$ is given by $\frac{1}{2}f_{\text{tot}}(x)$. The other half of $f_{\text{tot}}(x)$ results in charged leptons: electrons, muons, and taus. While electrons are stable, muons and taus decay further before interacting with the thermal bath.

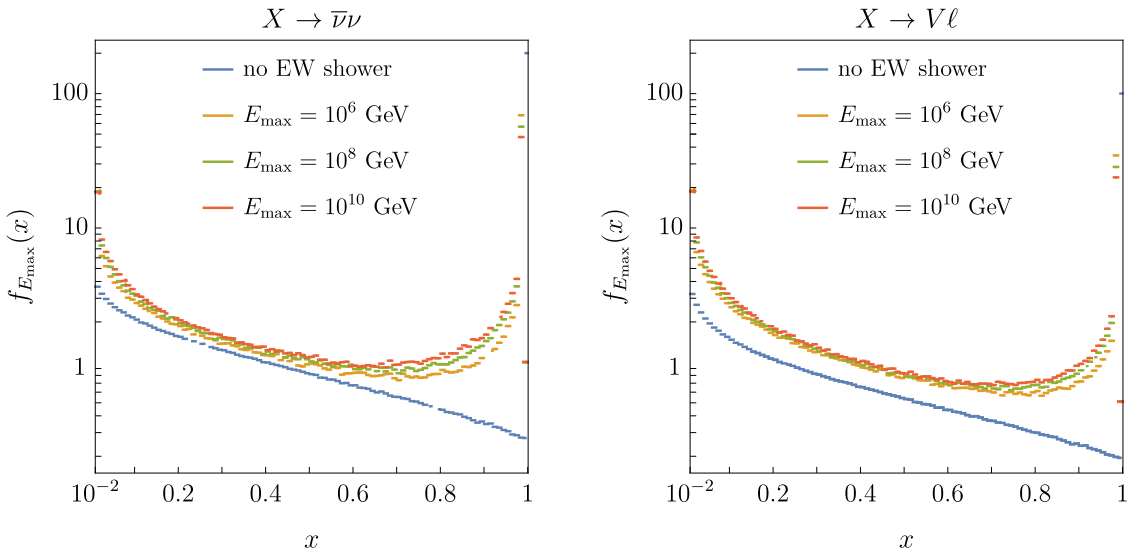

Figure 4.6: The final neutrino spectrum of decay model I and II considering EW showers at different energies. For comparison the spectrum without including EW showering is shown as well. The final spectrum includes decays to neutrinos from any gauge bosons, taus and muons produced in the EW shower or in the primary decay. We can see that for higher COM energies the peak decreases, which demonstrates how more energy is distributed to EW radiation.

Neutrinos from primary muon and tau decays will also contribute to the measured spectrum today. We assume an isotropic three-body decay, and decay all muons into three particles, two of which contribute to the neutrino spectrum. The tau-decays are more subtle as there is a greater variety of possible final states. We treat the leptonic tau decays in the same manner as the muon decays. We also include other tau-decays with up to three particles in the final state and add the resulting neutrinos to the spectrum, without further decaying any resulting mesons. The final neutrino spectrum, which is shown in Figure **??**, is denoted by $f_{E_{\max}}(x)$.

Neglecting hadronic decays may slightly underestimate the low energy tail of our distribution. In the future, it may be worth integrating an EW-shower formalism with a hadronic shower. For our purposes, the accuracy of the high energy tail of the neutrino distribution is most important, to which hadronic decays will not significantly contribute.

Bibliography

[1] M. Tanabashi, K. Hagiwara, K. Hikasa, K. Nakamura, Y. Sumino, F. Takahashi, J. Tanaka, K. Agashe, G. Aielli, C. Amsler, M. Antonelli, D. M. Asner, H. Baer, S. Banerjee, R. M. Barnett, T. Basaglia, C. W. Bauer, J. J. Beatty, V. I. Belousov, J. Beringer, S. Bethke, A. Bettini, H. Bichsel, O. Biebel, K. M. Black, E. Blucher, O. Buchmuller, V. Burkert, M. A. Bychkov, R. N. Cahn, M. Carena, A. Ceccucci, A. Cerri, D. Chakraborty, M.-C. Chen, R. S. Chivukula, G. Cowan, O. Dahl, G. D'Ambrosio, T. Damour, D. de Florian, A. de Gouvêa, T. DeGrand, P. de Jong, G. Dissertori, B. A. Dobrescu, M. D'Onofrio, M. Doser, M. Drees, H. K. Dreiner, D. A. Dwyer, P. Eerola, S. Eidelman, J. Ellis, J. Erler, V. V. Ezhela, W. Fetscher, B. D. Fields, R. Firestone, B. Foster, A. Freitas, H. Gallagher, L. Garren, H.-J. Gerber, G. Gerbier, T. Gershon, Y. Gershtein, T. Gherghetta, A. A. Godizov, M. Goodman, C. Grab, A. V. Gritsan, C. Grojean, D. E. Groom, M. Grünewald, A. Gurtu, T. Gutsche, H. E. Haber, C. Hanhart, S. Hashimoto, Y. Hayato, K. G. Hayes, A. Hebecker, S. Heinemeyer, B. Heltsley, J. J. Hernández-Rey, J. Hisano, A. Höcker, J. Holder, A. Holtkamp, T. Hyodo, K. D. Irwin, K. F. Johnson, M. Kado,

M. Karliner, U. F. Katz, S. R. Klein, E. Klempt, R. V. Kowalewski, F. Krauss, M. Kreps, B. Krusche, Y. V. Kuyanov, Y. Kwon, O. Lahav, J. Laiho, J. Lesgourgues, A. Liddle, Z. Ligeti, C.-J. Lin, C. Lippmann, T. M. Liss, L. Littenberg, K. S. Lugovsky, S. B. Lugovsky, A. Lusiani, Y. Makida, F. Maltoni, T. Mannel, A. V. Manohar, W. J. Marciano, A. D. Martin, A. Masoni, J. Matthews, U.-G. Meißner, D. Milstead, R. E. Mitchell, K. Mönig, P. Molaro, F. Moortgat, M. Moskovic, H. Murayama, M. Narain, P. Nason, S. Navas, M. Neubert, P. Nevski, Y. Nir, K. A. Olive, S. Pagan Griso, J. Parsons, C. Patrignani, J. A. Peacock, M. Pennington, S. T. Petcov, V. A. Petrov, E. Pianori, A. Piepke, A. Pomarol, A. Quadt, J. Rademacker, G. Raffelt, B. N. Ratcliff, P. Richardson, A. Ringwald, S. Roesler, S. Rolli, A. Romaniouk, L. J. Rosenberg, J. L. Rosner, G. Rybka, R. A. Ryutin, C. T. Sachrajda, Y. Sakai, G. P. Salam, S. Sarkar, F. Sauli, O. Schneider, K. Scholberg, A. J. Schwartz, D. Scott, V. Sharma, S. R. Sharpe, T. Shutt, M. Silari, T. Sjöstrand, P. Skands, T. Skwarnicki, J. G. Smith, G. F. Smoot, S. Spanier, H. Spieler, C. Spiering, A. Stahl, S. L. Stone, T. Sumiyoshi, M. J. Syphers, K. Terashi, J. Terning, U. Thoma, R. S. Thorne, L. Tiator, M. Titov, N. P. Tkachenko, N. A. Törnqvist, D. R. Tovey, G. Valencia, R. Van de Water, N. Varelas, G. Venanzoni, L. Verde, M. G. Vincter, P. Vogel, A. Vogt, S. P. Wakely, W. Walkowiak, C. W. Walter, D. Wands, D. R. Ward, M. O. Wascko, G. Weiglein, D. H. Weinberg, E. J. Weinberg, M. White, L. R. Wiencke, S. Willocq, C. G. Wohl, J. Womersley, C. L. Woody, R. L. Workman, W.-M. Yao, G. P. Zeller, O. V. Zenin, R.-Y. Zhu, S.-L. Zhu, F. Zimmermann, P. A. Zyla, J. Anderson, L. Fuller, V. S. Lugovsky, and

P. Schaffner, "Review of particle physics," *Phys. Rev. D*, vol. 98, p. 030001, Aug 2018. [Online]. Available: https://link.aps.org/doi/10.1103/PhysRevD.98.030001

[2] V. C. Rubin and J. Ford, W. Kent, "Rotation of the Andromeda Nebula from a Spectroscopic Survey of Emission Regions," ApJ, vol. 159, p. 379, Feb. 1970.

[3] V. C. Rubin, J. Ford, W. K., and N. Thonnard, "Rotational properties of 21 SC galaxies with a large range of luminosities and radii, from NGC 4605 (R=4kpc) to UGC 2885 (R=122kpc)." ApJ, vol. 238, pp. 471–487, Jun. 1980.

[4] A. G. Riess *et al.*, "Observational evidence from supernovae for an accelerating universe and a cosmological constant," *Astron. J.*, vol. 116, pp. 1009–1038, 1998.

[5] S. Perlmutter *et al.*, "Measurements of Ω and Λ from 42 high redshift supernovae," *Astrophys. J.*, vol. 517, pp. 565–586, 1999.

[6] D. N. Schramm and M. S. Turner, "Big-bang nucleosynthesis enters the precision era," *Rev. Mod. Phys.*, vol. 70, pp. 303–318, Jan 1998. [Online]. Available: https://link.aps.org/doi/10.1103/RevModPhys.70.303

[7] D. J. Eisenstein *et al.*, "Detection of the Baryon Acoustic Peak in the Large-Scale Correlation Function of SDSS Luminous Red Galaxies," *Astrophys. J.*, vol. 633, pp. 560–574, 2005.

[8] G. Hinshaw *et al.*, "Five-Year Wilkinson Microwave Anisotropy Probe (WMAP) Observations: Data Processing, Sky Maps, and Basic Results," *Astrophys. J. Suppl.*, vol. 180, pp. 225–245, 2009.

[9] C. Blake, E. A. Kazin, F. Beutler, T. M. Davis, D. Parkinson, S. Brough, M. Colless, C. Contreras, W. Couch, S. Croom, and et al., "The wigglez dark energy survey: mapping the distance-redshift relation with baryon acoustic oscillations," *Monthly Notices of the Royal Astronomical Society*, vol. 418, no. 3, p. 1707–1724, Oct 2011. [Online]. Available: http://dx.doi.org/10.1111/j.1365-2966.2011.19592.x

[10] C. L. Bennett, D. Larson, J. L. Weiland, N. Jarosik, G. Hinshaw, N. Odegard, K. M. Smith, R. S. Hill, B. Gold, M. Halpern, and et al., "Nine-year wilkinson microwave anisotropy probe (wmap) observations: Final maps and results," *The Astrophysical Journal Supplement Series*, vol. 208, no. 2, p. 20, Sep 2013. [Online]. Available: http://dx.doi.org/10.1088/0067-0049/208/2/20

[11] A. G. Riess *et al.*, "A 2.4% Determination of the Local Value of the Hubble Constant," *Astrophys. J.*, vol. 826, no. 1, p. 56, 2016.

[12] V. Bonvin, F. Courbin, S. H. Suyu, P. J. Marshall, C. E. Rusu, D. Sluse, M. Tewes, K. C. Wong, T. Collett, C. D. Fassnacht, T. Treu, M. W. Auger, S. Hilbert, L. V. E. Koopmans, G. Meylan, N. Rumbaugh, A. Sonnenfeld, and C. Spiniello, "H0LiCOW - V. New COSMOGRAIL time delays of HE 0435-1223: H_0 to 3.8 per cent precision from strong lensing in a flat ΛCDM model," MNRAS, vol. 465, no. 4, pp. 4914–4930, Mar. 2017.

[13] N. Aghanim *et al.*, "Planck 2018 results. VI. Cosmological parameters," 7 2018.

[14] A. G. Riess, "The Expansion of the Universe is Faster than Expected," *Nature Rev. Phys.*, vol. 2, no. 1, pp. 10–12, 2019.

[15] G. F. Smoot, C. L. Bennett, A. Kogut, E. L. Wright, J. Aymon, N. W. Boggess, E. S. Cheng, G. de Amici, S. Gulkis, M. G. Hauser, G. Hinshaw, P. D. Jackson, M. Janssen, E. Kaita, T. Kelsall, P. Keegstra, C. Lineweaver, K. Loewenstein, P. Lubin, J. Mather, S. S. Meyer, S. H. Moseley, T. Murdock, L. Rokke, R. F. Silverberg, L. Tenorio, R. Weiss, and D. T. Wilkinson, "Structure in the COBE Differential Microwave Radiometer First-Year Maps," ApJ, vol. 396, p. L1, Sep. 1992.

[16] F. Beutler, C. Blake, M. Colless, D. H. Jones, L. Staveley-Smith, L. Campbell, Q. Parker, W. Saunders, and F. Watson, "The 6df galaxy survey: baryon acoustic oscillations and the local hubble constant," *Monthly Notices of the Royal Astronomical Society*, vol. 416, no. 4, p. 3017–3032, Jul 2011. [Online]. Available: http://dx.doi.org/10.1111/j.1365-2966.2011.19250.x

[17] A. H. Guth, "Inflationary universe: A possible solution to the horizon and flatness problems," *Phys. Rev. D*, vol. 23, pp. 347–356, Jan 1981. [Online]. Available: https://link.aps.org/doi/10.1103/PhysRevD.23.347

[18] A. D. Linde, "A New Inflationary Universe Scenario: A Possible Solution of the Horizon, Flatness, Homogeneity, Isotropy and Primordial Monopole Problems," *Adv. Ser. Astrophys. Cosmol.*, vol. 3, pp. 149–153, 1987.

[19] K. V. Berghaus, P. W. Graham, and D. E. Kaplan, "Minimal Warm Inflation," 2019.

[20] J. L. Bernal, L. Verde, and A. G. Riess, "The trouble with H_0," *JCAP*, vol. 10, p. 019, 2016.

[21] J. Evslin, A. A. Sen, and Ruchika, "Price of shifting the Hubble constant," *Phys. Rev. D*, vol. 97, no. 10, p. 103511, 2018.

[22] W. L. Freedman, "Cosmology at a Crossroads," *Nature Astron.*, vol. 1, p. 0121, 2017.

[23] P. Ade *et al.*, "Planck 2015 results. XIII. Cosmological parameters," *Astron. Astrophys.*, vol. 594, p. A13, 2016.

[24] V. Poulin, T. L. Smith, T. Karwal, and M. Kamionkowski, "Early Dark Energy Can Resolve The Hubble Tension," *Phys. Rev. Lett.*, vol. 122, no. 22, p. 221301, 2019.

[25] K. V. Berghaus and T. Karwal, "Thermal Friction as a Solution to the Hubble Tension," *Phys. Rev. D*, vol. 101, no. 8, p. 083537, 2020.

[26] T. L. Smith, V. Poulin, and M. A. Amin, "Oscillating scalar fields and the Hubble tension: a resolution with novel signatures," 2019.

[27] K. V. Berghaus, M. D. Diamond, and D. Kaplan, "Decays of Long-Lived Relics and Their Signatures at IceCube," *JHEP*, vol. 05, p. 145, 2019.

[28] F. Halzen and S. R. Klein, "IceCube: An Instrument for Neutrino Astronomy," *Rev. Sci. Instrum.*, vol. 81, p. 081101, 2010.

[29] M. G. Aartsen *et al.*, "Evidence for High-Energy Extraterrestrial Neutrinos at the IceCube Detector," *Science*, vol. 342, p. 1242856, 2013.

[30] C. Kopper, W. Giang, and N. Kurahashi, "Observation of Astrophysical Neutrinos in Four Years of IceCube Data," *PoS*, vol. ICRC2015, p. 1081, 2016.

[31] C. Kopper, "Observation of Astrophysical Neutrinos in Six Years of IceCube Data," *PoS*, vol. ICRC2017, p. 981, 2018.

[32] M. G. Aartsen *et al.*, "Observation and Characterization of a Cosmic Muon Neutrino Flux from the Northern Hemisphere using six years of IceCube data," *Astrophys. J.*, vol. 833, no. 1, p. 3, 2016.

[33] B. Szczerbinska, R. Allahverdi, K. Babu, B. Balantekin, B. Dutta, T. Kamon, J. Kumar, F. Queiroz, L. Strigari, and R. Surman, Eds., *Proceedings, Workshop on Neutrino Physics : Session of CETUP* 2015 and 9th International Conference on Interconnections between Particle Physics and Cosmology (PPC2015)*, vol. 1743, 2016. [Online]. Available: http://aip.scitation.org/toc/apc/1743/1

[34] Y. Akrami *et al.*, "Planck 2018 results. X. Constraints on inflation," 2018.

[35] J. Martin, C. Ringeval, and V. Vennin, "Encyclopædia Inflationaris," *Phys. Dark Univ.*, vol. 5-6, pp. 75–235, 2014.

[36] S. Tsujikawa, J. Ohashi, S. Kuroyanagi, and A. De Felice, "Planck constraints on single-field inflation," *Phys. Rev.*, vol. D88, no. 2, p. 023529, 2013.

[37] A. Berera, "Warm inflation," *Phys. Rev. Lett.*, vol. 75, pp. 3218–3221, 1995.

[38] A. Berera and L.-Z. Fang, "Thermally induced density perturbations in the inflation era," *Phys. Rev. Lett.*, vol. 74, pp. 1912–1915, 1995.

[39] A. Berera, "Thermal properties of an inflationary universe," *Phys. Rev.*, vol. D54, pp. 2519–2534, 1996.

[40] ——, "Warm inflation at arbitrary adiabaticity: A Model, an existence proof for inflationary dynamics in quantum field theory," *Nucl. Phys.*, vol. B585, pp. 666–714, 2000.

[41] R. Rangarajan, "Current Status of Warm Inflation," in *Proceedings, 18th Lomonosov Conference on Elementary Particle Physics: Moscow, Russia, August 24-30, 2017*, 2019, pp. 339–345.

[42] M. Bastero-Gil and A. Berera, "Warm inflation model building," *Int. J. Mod. Phys.*, vol. A24, pp. 2207–2240, 2009.

[43] M. Bastero-Gil, A. Berera, I. G. Moss, and R. O. Ramos, "Theory of non-Gaussianity in warm inflation," *JCAP*, vol. 1412, no. 12, p. 008, 2014.

[44] J. Yokoyama and A. D. Linde, "Is warm inflation possible?" *Phys. Rev.*, vol. D60, p. 083509, 1999.

[45] I. G. Moss and C. Xiong, "Dissipation coefficients for supersymmetric inflatonary models," 2006.

[46] M. Bastero-Gil, A. Berera, R. O. Ramos, and J. G. Rosa, "Warm Little Inflaton," *Phys. Rev. Lett.*, vol. 117, no. 15, p. 151301, 2016.

[47] ——, "Towards a reliable effective field theory of inflation," 2019.

[48] L. Visinelli, "Natural Warm Inflation," *JCAP*, vol. 1109, p. 013, 2011.

[49] V. Kamali, "Warm (Pseudo)Scalar Inflation," 2019.

[50] G. D. Moore and M. Tassler, "The Sphaleron Rate in SU(N) Gauge Theory," *JHEP*, vol. 02, p. 105, 2011.

[51] L. Visinelli, "Observational Constraints on Monomial Warm Inflation," *JCAP*, vol. 1607, no. 07, p. 054, 2016.

[52] M. M. Anber and L. Sorbo, "Naturally inflating on steep potentials through electromagnetic dissipation," *Phys. Rev.*, vol. D81, p. 043534, 2010.

[53] ——, "Non-Gaussianities and chiral gravitational waves in natural steep inflation," *Phys. Rev.*, vol. D85, p. 123537, 2012.

[54] R. Z. Ferreira and A. Notari, "Thermalized axion inflation: natural and monomial inflation with small r," *Phys. Rev.*, vol. D97, no. 6, p. 063528, 2018.

[55] ——, "Thermalized Axion Inflation," *JCAP*, vol. 1709, no. 09, p. 007, 2017.

[56] H. Mishra, S. Mohanty, and A. Nautiyal, "Warm natural inflation," *Phys. Lett.*, vol. B710, pp. 245–250, 2012.

[57] C. Graham and I. G. Moss, "Density fluctuations from warm inflation," *JCAP*, vol. 0907, p. 013, 2009.

[58] M. Bastero-Gil, A. Berera, and R. O. Ramos, "Shear viscous effects on the primordial power spectrum from warm inflation," *JCAP*, vol. 1107, p. 030, 2011.

[59] A. R. Liddle and D. H. Lyth, *Cosmological inflation and large scale structure*, 2000.

[60] I. G. Moss and T. Yeomans, "Non-gaussianity in the strong regime of warm inflation," *JCAP*, vol. 1108, p. 009, 2011.

[61] P. A. R. Ade *et al.*, "Planck 2015 results. XVII. Constraints on primordial non-Gaussianity," *Astron. Astrophys.*, vol. 594, p. A17, 2016.

[62] I. G. Moss and C. Xiong, "Non-Gaussianity in fluctuations from warm inflation," *JCAP*, vol. 0704, p. 007, 2007.

[63] J. R. Fergusson and E. P. S. Shellard, "The shape of primordial non-Gaussianity and the CMB bispectrum," *Phys. Rev.*, vol. D80, p. 043510, 2009.

[64] K. N. Abazajian *et al.*, "CMB-S4 Science Book, First Edition," 2016.

[65] A. et. al, "Cosmology and fundamental physics with the euclid satellite," *Living Reviews in Relativity*, vol. 21, no. 1, p. 2, Apr 2018. [Online]. Available: https://doi.org/10.1007/s41114-017-0010-3

[66] O. Doré *et al.*, "Science Impacts of the SPHEREx All-Sky Optical to Near-Infrared Spectral Survey II: Report of a Community Workshop on the Scientific Synergies Between the SPHEREx Survey and Other Astronomy Observatories," 2018.

[67] D. J. Bacon *et al.*, "Cosmology with Phase 1 of the Square Kilometre Array: Red Book 2018: Technical specifications and performance forecasts," *Submitted to: Publ. Astron. Soc. Austral.*, 2018.

[68] D. Yamauchi, K. Takahashi, and M. Oguri, "Constraining primordial non-Gaussianity

via a multitracer technique with surveys by Euclid and the Square Kilometre Array," *Phys. Rev.*, vol. D90, no. 8, p. 083520, 2014.

[69] D. Karagiannis, A. Lazanu, M. Liguori, A. Raccanelli, N. Bartolo, and L. Verde, "Constraining primordial non-Gaussianity with bispectrum and power spectrum from upcoming optical and radio surveys," *Mon. Not. Roy. Astron. Soc.*, vol. 478, no. 1, pp. 1341–1376, 2018.

[70] D. J. Gross, R. D. Pisarski, and L. G. Yaffe, "Qcd and instantons at finite temperature," *Rev. Mod. Phys.*, vol. 53, pp. 43–80, Jan 1981. [Online]. Available: https://link.aps.org/doi/10.1103/RevModPhys.53.43

[71] J. Frison, R. Kitano, H. Matsufuru, S. Mori, and N. Yamada, "Topological susceptibility at high temperature on the lattice," *JHEP*, vol. 09, p. 021, 2016.

[72] P. Arnold and L. McLerran, "Sphalerons, small fluctuations, and baryon-number violation in electroweak theory," *Phys. Rev. D*, vol. 36, pp. 581–595, Jul 1987. [Online]. Available: https://link.aps.org/doi/10.1103/PhysRevD.36.581

[73] M. Laine and A. Vuorinen, "Basics of Thermal Field Theory," *Lect. Notes Phys.*, vol. 925, pp. pp.1–281, 2016.

[74] E. Masso, F. Rota, and G. Zsembinszki, "On axion thermalization in the early universe," *Phys. Rev.*, vol. D66, p. 023004, 2002.

[75] P. Graf and F. D. Steffen, "Thermal axion production in the primordial quark-gluon plasma," *Phys. Rev.*, vol. D83, p. 075011, 2011.

[76] R. O. Ramos and L. A. da Silva, "Power spectrum for inflation models with quantum and thermal noises," *JCAP*, vol. 1303, p. 032, 2013.

[77] A. D. Linde, "Hybrid inflation," *Phys. Rev.*, vol. D49, pp. 748–754, 1994.

[78] S. Bartrum, M. Bastero-Gil, A. Berera, R. Cerezo, R. O. Ramos, and J. G. Rosa, "The importance of being warm (during inflation)," *Phys. Lett.*, vol. B732, pp. 116–121, 2014.

[79] L. Visinelli, "Cosmological perturbations for an inflaton field coupled to radiation," *JCAP*, vol. 1501, no. 01, p. 005, 2015.

[80] A. G. Riess *et al.*, "Milky Way Cepheid Standards for Measuring Cosmic Distances and Application to Gaia DR2: Implications for the Hubble Constant," *Astrophys. J.*, vol. 861, no. 2, p. 126, 2018.

[81] L. Verde, T. Treu, and A. G. Riess, "Tensions between the Early and the Late Universe," in *Nature Astronomy 2019*, 2019.

[82] K. C. Wong *et al.*, "H0LiCOW XIII. A 2.4% measurement of H_0 from lensed quasars: 5.3σ tension between early and late-Universe probes," 2019.

[83] G. Efstathiou, "H0 Revisited," *Mon. Not. Roy. Astron. Soc.*, vol. 440, no. 2, pp. 1138–1152, 2014.

[84] G. E. Addison, Y. Huang, D. J. Watts, C. L. Bennett, M. Halpern, G. Hinshaw, and J. L. Weiland, "Quantifying discordance in the 2015 Planck CMB spectrum," *Astrophys. J.*, vol. 818, no. 2, p. 132, 2016.

[85] K. Aylor, M. Joy, L. Knox, M. Millea, S. Raghunathan, and W. L. K. Wu, "Sounds Discordant: Classical Distance Ladder & ΛCDM -based Determinations of the Cosmological Sound Horizon," *Astrophys. J.*, vol. 874, no. 1, p. 4, 2019.

[86] H. J. Macpherson, P. D. Lasky, and D. J. Price, "The trouble with Hubble: Local versus global expansion rates in inhomogeneous cosmological simulations with numerical relativity," *Astrophys. J.*, vol. 865, no. 1, p. L4, 2018.

[87] D. Camarena and V. Marra, "Impact of the cosmic variance on H_0 on cosmological analyses," *Phys. Rev.*, vol. D98, no. 2, p. 023537, 2018.

[88] D. O. Jones *et al.*, "Should Type Ia Supernova Distances be Corrected for their Local Environments?" *Astrophys. J.*, vol. 867, no. 2, p. 108, 2018.

[89] W. D. Kenworthy, D. Scolnic, and A. Riess, "The Local Perspective on the Hubble Tension: Local Structure Does Not Impact Measurement of the Hubble Constant," *Astrophys. J.*, vol. 875, no. 2, p. 145, 2019.

[90] B. Follin and L. Knox, "Insensitivity of the distance ladder Hubble constant determination to Cepheid calibration modelling choices," *Mon. Not. Roy. Astron. Soc.*, vol. 477, no. 4, pp. 4534–4542, 2018.

[91] D. N. Spergel, R. Flauger, and R. Hlozek, "Planck Data Reconsidered," *Phys. Rev.*, vol. D91, no. 2, p. 023518, 2015.

[92] S. M. Feeney, D. J. Mortlock, and N. Dalmasso, "Clarifying the Hubble constant

tension with a Bayesian hierarchical model of the local distance ladder," *Mon. Not. Roy. Astron. Soc.*, vol. 476, no. 3, pp. 3861–3882, 2018.

[93] S. Pandey, M. Raveri, and B. Jain, "A model independent comparison of supernova and strong lensing cosmography: implications for the Hubble constant tension," 2019.

[94] S. M. Feeney, D. J. Mortlock, and N. Dalmasso, "Clarifying the Hubble constant tension with a Bayesian hierarchical model of the local distance ladder," *Monthly Notices of the Royal Astronomical Society*, vol. 476, no. 3, pp. 3861–3882, 02 2018. [Online]. Available: https://doi.org/10.1093/mnras/sty418

[95] N. Blinov, K. J. Kelly, G. Z. Krnjaic, and S. D. McDermott, "Constraining the Self-Interacting Neutrino Interpretation of the Hubble Tension," 2019.

[96] L. Knox and M. Millea, "The Hubble Hunter's Guide," 2019.

[97] H. Desmond, B. Jain, and J. Sakstein, "Local resolution of the Hubble tension: The impact of screened fifth forces on the cosmic distance ladder," *Phys. Rev.*, vol. D100, no. 4, p. 043537, 2019.

[98] P. Agrawal, F.-Y. Cyr-Racine, D. Pinner, and L. Randall, "Rock 'n' Roll Solutions to the Hubble Tension," 2019.

[99] M.-X. Lin, G. Benevento, W. Hu, and M. Raveri, "Acoustic Dark Energy: Potential Conversion of the Hubble Tension," *Phys. Rev.*, vol. D100, no. 6, p. 063542, 2019.

[100] C. D. Kreisch, F.-Y. Cyr-Racine, and O. Doré, "The Neutrino Puzzle: Anomalies, Interactions, and Cosmological Tensions," 2019.

[101] T. Karwal and M. Kamionkowski, "Dark energy at early times, the Hubble parameter, and the string axiverse," *Phys. Rev.*, vol. D94, no. 10, p. 103523, 2016.

[102] S. Alexander and E. McDonough, "Axion-Dilaton Destabilization and the Hubble Tension," *Phys. Lett.*, vol. B797, p. 134830, 2019.

[103] F. Niedermann and M. S. Sloth, "New Early Dark Energy," 2019.

[104] J. Sakstein and M. Trodden, "Early dark energy from massive neutrinos – a natural resolution of the Hubble tension," 2019.

[105] L. McLerran, E. Mottola, and M. E. Shaposhnikov, "Sphalerons and axion dynamics in high-temperature qcd," *Phys. Rev. D*, vol. 43, pp. 2027–2035, Mar 1991. [Online]. Available: https://link.aps.org/doi/10.1103/PhysRevD.43.2027

[106] A. Berera, M. Gleiser, and R. O. Ramos, "A First principles warm inflation model that solves the cosmological horizon / flatness problems," *Phys. Rev. Lett.*, vol. 83, pp. 264–267, 1999.

[107] A. Berera, I. G. Moss, and R. O. Ramos, "Warm Inflation and its Microphysical Basis," *Rept. Prog. Phys.*, vol. 72, p. 026901, 2009.

[108] W. Hu, M. Fukugita, M. Zaldarriaga, and M. Tegmark, "CMB observables and their cosmological implications," *Astrophys. J.*, vol. 549, p. 669, 2001.

[109] J. Lesgourgues, "The cosmic linear anisotropy solving system (class) i: Overview," 2011.

[110] D. Blas, J. Lesgourgues, and T. Tram, "The cosmic linear anisotropy solving system (class). part ii: Approximation schemes," *Journal of Cosmology and Astroparticle Physics*, vol. 2011, no. 07, p. 034–034, Jul 2011. [Online]. Available: http://dx.doi.org/10.1088/1475-7516/2011/07/034

[111] W. Hu, "Structure formation with generalized dark matter," *Astrophys. J.*, vol. 506, pp. 485–494, 1998.

[112] E. V. Linder and T. L. Smith, "Dark Before Light: Testing the Cosmic Expansion History through the Cosmic Microwave Background," *JCAP*, vol. 1104, p. 001, 2011.

[113] B. Follin, L. Knox, M. Millea, and Z. Pan, "First Detection of the Acoustic Oscillation Phase Shift Expected from the Cosmic Neutrino Background," *Phys. Rev. Lett.*, vol. 115, no. 9, p. 091301, 2015.

[114] P. W. Graham, D. E. Kaplan, and S. Rajendran, "Relaxation of the Cosmological Constant," *Phys. Rev.*, vol. D100, no. 1, p. 015048, 2019.

[115] M. Kamionkowski, J. Pradler, and D. G. E. Walker, "Dark energy from the string axiverse," *Phys. Rev. Lett.*, vol. 113, no. 25, p. 251302, 2014.

[116] V. Poulin, T. L. Smith, D. Grin, T. Karwal, and M. Kamionkowski, "Cosmological implications of ultralight axionlike fields," *Phys. Rev.*, vol. D98, no. 8, p. 083525, 2018.

[117] M. G. Aartsen *et al.*, "Observation of High-Energy Astrophysical Neutrinos in Three Years of IceCube Data," *Phys. Rev. Lett.*, vol. 113, p. 101101, 2014.

[118] ——, "All-sky Search for Time-integrated Neutrino Emission from Astrophysical Sources with 7 yr of IceCube Data," *Astrophys. J.*, vol. 835, no. 2, p. 151, 2017.

[119] ——, "Multimessenger observations of a flaring blazar coincident with high-energy neutrino IceCube-170922A," *Science*, vol. 361, no. 6398, p. eaat1378, 2018.

[120] W. Essey, O. Kalashev, A. Kusenko, and J. F. Beacom, "Role of line-of-sight cosmic ray interactions in forming the spectra of distant blazars in TeV gamma rays and high-energy neutrinos," *Astrophys. J.*, vol. 731, p. 51, 2011.

[121] O. E. Kalashev, A. Kusenko, and W. Essey, "PeV neutrinos from intergalactic interactions of cosmic rays emitted by active galactic nuclei," *Phys. Rev. Lett.*, vol. 111, no. 4, p. 041103, 2013.

[122] F. W. Stecker, "Limiting superluminal electron and neutrino velocities using the 2010 Crab Nebula flare and the IceCube PeV neutrino events," *Astropart. Phys.*, vol. 56, pp. 16–18, 2014.

[123] I. Tamborra, S. Ando, and K. Murase, "Star-forming galaxies as the origin of diffuse high-energy backgrounds: Gamma-ray and neutrino connections, and implications for starburst history," *JCAP*, vol. 1409, p. 043, 2014.

[124] K. Murase, M. Ahlers, and B. C. Lacki, "Testing the Hadronuclear Origin of PeV Neutrinos Observed with IceCube," *Phys. Rev.*, vol. D88, no. 12, p. 121301, 2013.

[125] C. Lunardini, S. Razzaque, K. T. Theodoseau, and L. Yang, "Neutrino Events at IceCube and the Fermi Bubbles," *Phys. Rev.*, vol. D90, no. 2, p. 023016, 2014.

[126] C. D. Dermer, K. Murase, and Y. Inoue, "Photopion Production in Black-Hole Jets and Flat-Spectrum Radio Quasars as PeV Neutrino Sources," *JHEAp*, vol. 3-4, pp. 29–40, 2014.

[127] P. Padovani and E. Resconi, "Are both BL Lacs and pulsar wind nebulae the astrophysical counterparts of IceCube neutrino events?" *Mon. Not. Roy. Astron. Soc.*, vol. 443, no. 1, pp. 474–484, 2014.

[128] K. Murase, Y. Inoue, and C. D. Dermer, "Diffuse Neutrino Intensity from the Inner Jets of Active Galactic Nuclei: Impacts of External Photon Fields and the Blazar Sequence," *Phys. Rev.*, vol. D90, no. 2, p. 023007, 2014.

[129] Y. Bai, R. Lu, and J. Salvado, "Geometric Compatibility of IceCube TeV-PeV Neutrino Excess and its Galactic Dark Matter Origin," *JHEP*, vol. 01, p. 161, 2016.

[130] A. Esmaili and P. D. Serpico, "Are IceCube neutrinos unveiling PeV-scale decaying dark matter?" *JCAP*, vol. 1311, p. 054, 2013.

[131] C. Rott, K. Kohri, and S. C. Park, "Superheavy dark matter and IceCube neutrino signals: Bounds on decaying dark matter," *Phys. Rev.*, vol. D92, no. 2, p. 023529, 2015.

[132] A. Esmaili, S. K. Kang, and P. D. Serpico, "IceCube events and decaying dark matter: hints and constraints," *JCAP*, vol. 1412, no. 12, p. 054, 2014.

[133] K. Murase, R. Laha, S. Ando, and M. Ahlers, "Testing the Dark Matter Scenario for

PeV Neutrinos Observed in IceCube," *Phys. Rev. Lett.*, vol. 115, no. 7, p. 071301, 2015.

[134] P. Ko and Y. Tang, "IceCube Events from Heavy DM decays through the Right-handed Neutrino Portal," *Phys. Lett.*, vol. B751, pp. 81–88, 2015.

[135] T. Cohen, K. Murase, N. L. Rodd, B. R. Safdi, and Y. Soreq, "γ-ray Constraints on Decaying Dark Matter and Implications for IceCube," *Phys. Rev. Lett.*, vol. 119, no. 2, p. 021102, 2017.

[136] P. S. B. Dev, D. Kazanas, R. N. Mohapatra, V. L. Teplitz, and Y. Zhang, "Heavy right-handed neutrino dark matter and PeV neutrinos at IceCube," *JCAP*, vol. 1608, no. 08, p. 034, 2016.

[137] A. Bhattacharya, A. Esmaili, S. Palomares-Ruiz, and I. Sarcevic, "Probing decaying heavy dark matter with the 4-year IceCube HESE data," *JCAP*, vol. 1707, no. 07, p. 027, 2017.

[138] D. Borah, A. Dasgupta, U. K. Dey, S. Patra, and G. Tomar, "Multi-component Fermionic Dark Matter and IceCube PeV scale Neutrinos in Left-Right Model with Gauge Unification," *JHEP*, vol. 09, p. 005, 2017.

[139] Y. Sui and P. S. Bhupal Dev, "A Combined Astrophysical and Dark Matter Interpretation of the IceCube HESE and Throughgoing Muon Events," *JCAP*, vol. 1807, no. 07, p. 020, 2018.

[140] M. G. Aartsen *et al.*, "Search for neutrinos from decaying dark matter with IceCube,"

Eur. Phys. J., vol. C78, no. 10, p. 831, 2018.

[141] A. Esmaili and P. D. Serpico, "Gamma-ray bounds from EAS detectors and heavy decaying dark matter constraints," *JCAP*, vol. 1510, no. 10, p. 014, 2015.

[142] P. Ciafaloni, D. Comelli, A. Riotto, F. Sala, A. Strumia, and A. Urbano, "Weak Corrections are Relevant for Dark Matter Indirect Detection," *JCAP*, vol. 1103, p. 019, 2011.

[143] J. Chen, T. Han, and B. Tweedie, "Electroweak Splitting Functions and High Energy Showering," *JHEP*, vol. 11, p. 093, 2017.

[144] S. Sarkar and R. Toldra, "The High-energy cosmic ray spectrum from relic particle decay," *Nucl. Phys.*, vol. B621, pp. 495–520, 2002.

[145] C. Barbot and M. Drees, "Production of ultraenergetic cosmic rays through the decay of superheavy X particles," *Phys. Lett.*, vol. B533, pp. 107–115, 2002.

[146] P. Ciafaloni, M. Cirelli, D. Comelli, A. De Simone, A. Riotto, and A. Urbano, "On the Importance of Electroweak Corrections for Majorana Dark Matter Indirect Detection," *JCAP*, vol. 1106, p. 018, 2011.

[147] L. A. Cavasonza, M. Krämer, and M. Pellen, "Electroweak fragmentation functions for dark matter annihilation," *JCAP*, vol. 1502, no. 02, p. 021, 2015.

[148] Y. Ema, R. Jinno, and T. Moroi, "Cosmic-Ray Neutrinos from the Decay of Long-Lived Particle and the Recent IceCube Result," *Phys. Lett.*, vol. B733, pp. 120–125, 2014.

[149] ——, "Cosmological Implications of High-Energy Neutrino Emission from the Decay of Long-Lived Particle," *JHEP*, vol. 10, p. 150, 2014.

[150] A. Esmaili, A. Ibarra, and O. L. G. Peres, "Probing the stability of superheavy dark matter particles with high-energy neutrinos," *JCAP*, vol. 1211, p. 034, 2012.

[151] G. Kane, K. Sinha, and S. Watson, "Cosmological Moduli and the Post-Inflationary Universe: A Critical Review," *Int. J. Mod. Phys.*, vol. D24, no. 08, p. 1530022, 2015.

[152] K. Kainulainen, S. Nurmi, T. Tenkanen, K. Tuominen, and V. Vaskonen, "Isocurvature Constraints on Portal Couplings," *JCAP*, vol. 1606, no. 06, p. 022, 2016.

[153] M. Heikinheimo, T. Tenkanen, K. Tuominen, and V. Vaskonen, "Observational Constraints on Decoupled Hidden Sectors," *Phys. Rev.*, vol. D94, no. 6, p. 063506, 2016, [Erratum: Phys. Rev.D96,no.10,109902(2017)].

[154] M. Boudaud, M. Cirelli, G. Giesen, and P. Salati, "A fussy revisitation of antiprotons as a tool for Dark Matter searches," *JCAP*, vol. 1505, no. 05, p. 013, 2015.

[155] P. B. Denton, D. Marfatia, and T. J. Weiler, "The Galactic Contribution to IceCube's Astrophysical Neutrino Flux," *JCAP*, vol. 1708, no. 08, p. 033, 2017.

[156] M. Tanabashi, K. Hagiwara, K. Hikasa, K. Nakamura, Y. Sumino, F. Takahashi, J. Tanaka, K. Agashe, G. Aielli, C. Amsler, M. Antonelli, D. M. Asner, H. Baer, S. Banerjee, R. M. Barnett, T. Basaglia, C. W. Bauer, J. J. Beatty, V. I. Belousov, J. Beringer, S. Bethke, A. Bettini, H. Bichsel, O. Biebel, K. M. Black, E. Blucher, O. Buchmuller, V. Burkert, M. A. Bychkov, R. N. Cahn, M. Carena, A. Ceccucci,

BIBLIOGRAPHY

A. Cerri, D. Chakraborty, M.-C. Chen, R. S. Chivukula, G. Cowan, O. Dahl, G. D'Ambrosio, T. Damour, D. de Florian, A. de Gouvêa, T. DeGrand, P. de Jong, G. Dissertori, B. A. Dobrescu, M. D'Onofrio, M. Doser, M. Drees, H. K. Dreiner, D. A. Dwyer, P. Eerola, S. Eidelman, J. Ellis, J. Erler, V. V. Ezhela, W. Fetscher, B. D. Fields, R. Firestone, B. Foster, A. Freitas, H. Gallagher, L. Garren, H.-J. Gerber, G. Gerbier, T. Gershon, Y. Gershtein, T. Gherghetta, A. A. Godizov, M. Goodman, C. Grab, A. V. Gritsan, C. Grojean, D. E. Groom, M. Grünewald, A. Gurtu, T. Gutsche, H. E. Haber, C. Hanhart, S. Hashimoto, Y. Hayato, K. G. Hayes, A. Hebecker, S. Heinemeyer, B. Heltsley, J. J. Hernández-Rey, J. Hisano, A. Höcker, J. Holder, A. Holtkamp, T. Hyodo, K. D. Irwin, K. F. Johnson, M. Kado, M. Karliner, U. F. Katz, S. R. Klein, E. Klempt, R. V. Kowalewski, F. Krauss, M. Kreps, B. Krusche, Y. V. Kuyanov, Y. Kwon, O. Lahav, J. Laiho, J. Lesgourgues, A. Liddle, Z. Ligeti, C.-J. Lin, C. Lippmann, T. M. Liss, L. Littenberg, K. S. Lugovsky, S. B. Lugovsky, A. Lusiani, Y. Makida, F. Maltoni, T. Mannel, A. V. Manohar, W. J. Marciano, A. D. Martin, A. Masoni, J. Matthews, U.-G. Meißner, D. Milstead, R. E. Mitchell, K. Mönig, P. Molaro, F. Moortgat, M. Moskovic, H. Murayama, M. Narain, P. Nason, S. Navas, M. Neubert, P. Nevski, Y. Nir, K. A. Olive, S. Pagan Griso, J. Parsons, C. Patrignani, J. A. Peacock, M. Pennington, S. T. Petcov, V. A. Petrov, E. Pianori, A. Piepke, A. Pomarol, A. Quadt, J. Rademacker, G. Raffelt, B. N. Ratcliff, P. Richardson, A. Ringwald, S. Roesler, S. Rolli, A. Romaniouk, L. J. Rosenberg, J. L. Rosner, G. Rybka, R. A. Ryutin, C. T. Sachrajda, Y. Sakai, G. P. Salam, S. Sarkar, F. Sauli, O. Schneider, K. Scholberg,

A. J. Schwartz, D. Scott, V. Sharma, S. R. Sharpe, T. Shutt, M. Silari, T. Sjöstrand, P. Skands, T. Skwarnicki, J. G. Smith, G. F. Smoot, S. Spanier, H. Spieler, C. Spiering, A. Stahl, S. L. Stone, T. Sumiyoshi, M. J. Syphers, K. Terashi, J. Terning, U. Thoma, R. S. Thorne, L. Tiator, M. Titov, N. P. Tkachenko, N. A. Törnqvist, D. R. Tovey, G. Valencia, R. Van de Water, N. Varelas, G. Venanzoni, L. Verde, M. G. Vincter, P. Vogel, A. Vogt, S. P. Wakely, W. Walkowiak, C. W. Walter, D. Wands, D. R. Ward, M. O. Wascko, G. Weiglein, D. H. Weinberg, E. J. Weinberg, M. White, L. R. Wiencke, S. Willocq, C. G. Wohl, J. Womersley, C. L. Woody, R. L. Workman, W.-M. Yao, G. P. Zeller, O. V. Zenin, R.-Y. Zhu, S.-L. Zhu, F. Zimmermann, P. A. Zyla, J. Anderson, L. Fuller, V. S. Lugovsky, and P. Schaffner, "Review of particle physics," *Phys. Rev. D*, vol. 98, p. 030001, Aug 2018. [Online]. Available: https://link.aps.org/doi/10.1103/PhysRevD.98.030001

[157] M. Kawasaki and T. Moroi, "Gravitino production in the inflationary universe and the effects on big bang nucleosynthesis," *Prog. Theor. Phys.*, vol. 93, pp. 879–900, 1995.

[158] K. Jedamzik, "Big bang nucleosynthesis constraints on hadronically and electromagnetically decaying relic neutral particles," *Phys. Rev.*, vol. D74, p. 103509, 2006.

[159] R. H. Cyburt, J. R. Ellis, B. D. Fields, and K. A. Olive, "Updated nucleosynthesis constraints on unstable relic particles," *Phys. Rev.*, vol. D67, p. 103521, 2003.

[160] M. Kawasaki and T. Moroi, "Electromagnetic cascade in the early universe and its application to the big bang nucleosynthesis," *Astrophys. J.*, vol. 452, p. 506, 1995.

[161] R. J. Protheroe, T. Stanev, and V. S. Berezinsky, "Electromagnetic cascades and cascade nucleosynthesis in the early universe," *Phys. Rev.*, vol. D51, pp. 4134–4144, 1995.

[162] V. Poulin and P. D. Serpico, "Nonuniversal BBN bounds on electromagnetically decaying particles," *Phys. Rev.*, vol. D91, no. 10, p. 103007, 2015.

[163] V. Poulin, J. Lesgourgues, and P. D. Serpico, "Cosmological constraints on exotic injection of electromagnetic energy," *JCAP*, vol. 1703, no. 03, p. 043, 2017.

[164] T. R. Slatyer and C.-L. Wu, "General Constraints on Dark Matter Decay from the Cosmic Microwave Background," *Phys. Rev.*, vol. D95, no. 2, p. 023010, 2017.

[165] A. Kogut *et al.*, "The Primordial Inflation Explorer (PIXIE): A Nulling Polarimeter for Cosmic Microwave Background Observations," *JCAP*, vol. 1107, p. 025, 2011.

[166] A. A. Zdziarski and R. Svensson, "Absorption of X-rays and gamma rays at cosmological distances," *apj*, vol. 344, pp. 551–566, sep 1989.

[167] M. Ackermann *et al.*, "The spectrum of isotropic diffuse gamma-ray emission between 100 MeV and 820 GeV," *Astrophys. J.*, vol. 799, p. 86, 2015.

[168] G. D. Kribs and I. Z. Rothstein, "Bounds on longlived relics from diffuse gamma-ray observations," *Phys. Rev.*, vol. D55, pp. 4435–4449, 1997, [Erratum: Phys. Rev.D56,1822(1997)].

[169] A. A. Zdziarski, "Saturated pair-photon cascades on isotropic background photons," *apj*, vol. 335, pp. 786–802, dec 1988.

[170] J. Chluba, "Science with CMB spectral distortions," in *Proceedings, 49th Rencontres de Moriond on Cosmology: La Thuile, Italy, March 15-22, 2014*, 2014, pp. 327–334.

[171] W. Hu and J. Silk, "Thermalization constraints and spectral distortions for massive unstable relic particles," *Phys. Rev. Lett.*, vol. 70, pp. 2661–2664, May 1993. [Online]. Available: https://link.aps.org/doi/10.1103/PhysRevLett.70.2661

[172] D. J. Fixsen, E. S. Cheng, J. M. Gales, J. C. Mather, R. A. Shafer, and E. L. Wright, "The Cosmic Microwave Background spectrum from the full COBE FIRAS data set," *Astrophys. J.*, vol. 473, p. 576, 1996.

[173] J. D. Bowman, A. E. E. Rogers, R. A. Monsalve, T. J. Mozdzen, and N. Mahesh, "An absorption profile centred at 78 megahertz in the sky-averaged spectrum," *Nature*, vol. 555, no. 7694, pp. 67–70, 2018.

[174] E. D. Kovetz, I. Cholis, and D. E. Kaplan, "Bounds on Ultra-Light Hidden-Photon Dark Matter from 21cm at Cosmic Dawn," 2018.

[175] R. Barkana, N. J. Outmezguine, D. Redigolo, and T. Volansky, "Signs of Dark Matter at 21-cm?" 2018.

[176] D. B. Fox, K. Kashiyama, and P. Mészarós, "Sub-PeV Neutrinos from TeV Unidentified Sources in the Galaxy," *Astrophys. J.*, vol. 774, p. 74, 2013.

[177] M. G. Aartsen *et al.*, "IceCube-Gen2: A Vision for the Future of Neutrino Astronomy in Antarctica," 2014.

[178] M. Di Mauro, "The origin of the Fermi-LAT γ-ray background," in *Proceedings, 14th*

Marcel Grossmann Meeting on Recent Developments in Theoretical and Experimental General Relativity, Astrophysics, and Relativistic Field Theories (MG14) (In 4 Volumes): Rome, Italy, July 12-18, 2015, vol. 3, 2017, pp. 3098–3104.

[179] J. Knödlseder, "The future of gamma-ray astronomy," *Comptes Rendus Physique*, vol. 17, pp. 663–678, 2016.

Vita

Kim V. Berghaus was born in Frankurt, Germany on August 18, 1992. Playing competitive tennis throughout her youth, she obtained a full athletic scholarship for her bachelor studies in the United States. Graduating Magna Cum Laude with a B.S. in physics from UMBC, she received the Mulligan Memorial Fellowship, the outstanding senior in physics award, and the Matt Skalsky outstanding scholar athlete award. Gaining inital research experience with Prof. Michael Hayden and Dr. Giuliano Scarcelli in nonlinear and biomedical optics respectively, she joined the Department of Physics & Astronomy at Johns Hopkins University in 2015 to obtain her PhD in theoretical particle physics under the advisement of Prof. David E. Kaplan, where she was awarded the Gardner Fellowship in 2017. Following the completion of her PhD studies in 2020, she will continue her research in particle physics at YITP, Stonybrook.

VITA